UNIVERSITY OF HELSINKI REPORT SERIES IN PHYSICS

HU-P-D103

FIR 1 EPITHERMAL NEUTRON BEAM MODEL AND DOSE CALCULATION FOR TREATMENT PLANNING IN NEUTRON CAPTURE THERAPY

TIINA SEPPÄLÄ

Department of Physical Sciences
Faculty of Science
University of Helsinki
Helsinki, Finland

Helsinki 2002

UNIVERSITY OF HELSINKI REPORT SERIES IN PHYSICS

HU-P-D103

FIR 1 EPITHERMAL NEUTRON BEAM MODEL AND DOSE CALCULATION FOR TREATMENT PLANNING IN NEUTRON CAPTURE THERAPY

Tiina Seppälä

Department of Physical Sciences
Faculty of Science
University of Helsinki
Helsinki, Finland

ACADEMIC DISSERTATION

To be presented, with the permission of the Faculty of Science of the University of Helsinki, for public criticism in the Auditorium D101, Physicum, on December 13th, 2002, at 13 o'clock.

Helsinki 2002

ISBN 952-10-0569-6 (printed version)
ISSN 0356-0961
Helsinki 2002
Yliopistopaino

ISBN 952-10-0570-X (PDF version)
http://ethesis.helsinki.fi/
Helsinki 2002
Helsingin yliopiston verkkojulkaisut

T. Seppälä: FiR 1 epithermal neutron beam model and dose calculation for treatment planning in neutron capture therapy, University of Helsinki, 2002, 46 p.+appendices, University of Helsinki, Report Series in Physics, HU-P-D103, ISSN 0356-0961, ISBN 952-10-0569-6.

Classification (INSPEC): C7320, A8770H, A8760M, B7500, A8760J
Keywords: radiation therapy, BNCT, epithermal neutrons, dosimetry

ABSTRACT

The epithermal neutron beam model of the Finnish boron neutron capture therapy (BNCT) facility (FiR 1) was created using the two-dimensional (2D) discrete ordinates transport (DORT) code. The final design of the beam was achieved using the DORT model: the optimal thickness of the neutron moderator and the length and the thickness of the bismuth collimator of the beam were calculated. The final beam model was validated experimentally with dosimetric measurements. The computed neutron beam spectrum was first verified with activation measurements free in air. Suitable brain tissue substitutes for neutron capture therapy (NCT) dosimetry were examined. The computed thermal neutron fluence [and gold (Au) and manganese (Mn) activation reaction rates], the gamma dose and the fast neutron dose distributions in the three tissue substitute (TS) phantoms were verified with activation and pair ionisation chamber measurements. The simplified neutron-photon beam model for the treatment planning system (TPS) was determined from the DORT model. The TPS beam model was experimentally validated in the three TS phantoms. The beam model was normalised to the Au activation measurements at the thermal neutron maximum in the PMMA (polymethylmethacrylate) phantom, which gave a link to the monitor units. The planned radiation dose in the TPS is given in monitor units. The experimentally verified beam model was first applied in the computations of the dose plans of the dog brain and in the treatment planning of glioblastoma multiforme (GBM) patients in the Finnish BNCT project.

The 2D cylinder symmetrical horizontal DORT model of the FiR 1 epithermal neutron beam was observed to be an effective and reliable tool for examining the effects of different geometrical structures (moderator, collimator) on neutron and photon spectra. Of the simple phantom materials, PMMA was found to simulate the thermal neutron fluence at its maximum in the brain tissue 3 percentage units closer than water in the collimated epithermal neutron beam. However, water simulated the absorbed gamma dose in the brain tissue 12 percentage units closer than PMMA. In addition, a brain tissue equivalent liquid was designed. Parallel verification of the beam model in water, PMMA and the brain equivalent liquid confirmed reliability of the NCT dose computation. The DORT beam model was sufficiently accurate (intensity correction 5%) to use as a beam model in TPS. The beam model was normalised at the thermal neutron maximum in the PMMA phantom with the Au activation measurements. The use of the calculated Au activation reaction rate (variation 3%) for the normalisation was found to be less independent of the energy grouping of cross sections than the calculated Mn activation reaction rate (variation 13%).

The soft tissue, bone and air cavities need to be defined separately to create an accurate three-dimensional (3D) head model of the target area for the BNCT treatment planning. The accuracy of the beam model can be roughly estimated with *in vivo* dosimetry, which is recommended for use at epithermal neutron facilities in accordance with new protocols. The

total uncertainty of the computed total absorbed BNCT dose at the dose maximum in the brain tissue was estimated to be 8% (1SD) without uncertainty in boron concentration. The uncertainty of the computed NCT doses arises mostly from uncertainties in measured doses, thus, the uncertainty of the computed doses can be enhanced significantly by developing measurement techniques.

CONTENTS

LIST OF PUBLICATIONS:

This thesis is based on the following studies which are referred to in the text by their Roman numerals:

I Serén, T., Auterinen, I., Seppälä, T. and Kotiluoto, P. Spectrum measurements and calculations in the epithermal neutron beam at the FiR 1 BNCT facility. In: 15th European TRIGA Conference, VTT Symposium 197. Salmenhaara S. (ed.), pp. 167-79. Espoo: Libella (1999).

II Seppälä, T., Vähätalo, J., Auterinen, I., Kosunen, A., Nigg, D.W., Wheeler, F.J. and Savolainen, S. Modelling of brain tissue substitutes for phantom materials in neutron capture therapy (NCT) dosimetry. Radiat. Phys. Chem. 55, 239-46 (1999).

III Kosunen, A., Kortesniemi, M., Ylä-Mella, H., Seppälä, T., Lampinen, J., Serén, T., Auterinen, I., Järvinen, H. and Savolainen, S. Twin ionisation chambers for dose determinations in phantom in an epithermal neutron beam. Radiat. Prot. Dosim. 81, 187-94 (1999).

IV Seppälä, T., Serén, T. and Auterinen, I. Source characterisation for the rtt_MC treatment planning program at FiR 1. In: Frontiers in Neutron Capture Therapy, Vol. 1. Hawthorne M.F., Shelly K., Wiersema R.J. (eds.), pp. 219-24. New York: Plenum Publishers (2001).

V Aschan, C., Toivonen, M, Savolainen, S., Seppälä, T. and Auterinen, I. Epithermal neutron beam dosimetry with thermoluminescence dosemeters for boron neutron capture therapy. Radiat. Prot. Dosim. 81, 47-56 (1999).

VI Seppälä, T., Auterinen, I., Aschan, C., Serén, T., Benczik, J., Snellman, M., Huiskamp, R., Abo Ramadan, U., Kankaanranta, L., Joensuu, H. and Savolainen S. Dose planning with comparison to *in vivo* dosimetry for epithermal neutron irradiation of the dog brain. Med. Phys. 29, 2629-40 (2002).

VII Seppälä, T., Kotiluoto, P., Savolainen, S., Auterinen, I., Hiismäki, P., Serén, T., Kosunen, A., Aschan, C., Kortesniemi, M. and Toivonen, M. Determining and reporting the doses in the treatments of glioma patients in the epithermal neutron beam at the Finnish BNCT facility (FiR 1). IAEA-TECDOC-1223, 275-87 (2001).

Statement of involvement

All publications included in this thesis are a result of a group effort. In Study I, the author (T. Seppälä) constructed and described the DORT model of the FiR 1 epithermal neutron beam and computed the neutron spectra. In Study II, the author designed, implemented and analysed the computations. In Study III, the author computed the neutron spectra and the doses in the phantoms. In Study IV, the author defined the beam model for the TPS and implemented the validation and normalisation of the beam model. In Study V, the author computed the neutron spectra and the doses in the phantoms. In Study VI, the author helped design the dose planning set-up, implemented the dose plans and estimated the uncertainties of the computations. In Study VII, the author implemented the computational dosimetry and treatment planning. Moreover, Studies II, IV, VI and VII were written by the author of this thesis.

LIST OF SYMBOLS AND ABBREVIATIONS

A-150	Plastic substitute material for tissue
ANISN	One-dimensional discrete ordinates transport code system with anisotropic scattering
BMRR	Brookhaven Medical Research Reactor located in New York, USA
BNCT	Boron neutron capture therapy
BNCT_Rtpe	BNCT radiation treatment planning environment
BPA-F	Boronphenylalanine-fructose
BUGLE-80	Coupled 47 neutron, 20 gamma-ray group, P3, cross section library for light water reactor shielding calculations
C/E	Ratio of calculated and experimental values
$c_{B,blood}$	^{10}B concentration in blood
Cross section	Probability of a given type of interaction for the target nucleus concerned
CT	Computed tomography
D_g	Total absorbed gamma dose
D_n	Total absorbed neutron dose
D_N	Absorbed dose from the nitrogen capture reaction
$D_{g,H}$	Absorbed gamma dose from the hydrogen capture reaction
$D_{g,capture}$	Absorbed gamma dose from the capture reactions
$D_{g,beam}$	Absorbed gamma dose from photons in the beam
D_{fast_n}	Absorbed fast neutron dose predominantly from recoil protons
D_W	Total weighted dose
$\dot{D}^{calc}_{\mathrm{Re}f}$	Calculated dose rate at the reference monitor unit rate
DORT	Two-dimensional discrete ordinates transport code
E	Energy
ENDF/B	Evaluated nuclear data file cross section library
$f_n(E)$	Neutron kerma factor or fluence-to-kerma factor
$f_{B,ppm}$	^{10}B kerma factor for 1 ppm ^{10}B concentration
f_N	Nitrogen kerma factor
f_{fast_n}	Fast neutron kerma factor
$\phi(E)$	Neutron fluence rate
Φ_{th}	Thermal neutron fluence
FiR 1	Finnish research reactor located in Otaniemi, Espoo
FiR(K63)	Collimated epithermal neutron beam with 63-cm-long moderator at FiR 1
FiR(K75)	Collimated epithermal neutron beam with 75-cm-long moderator at FiR 1
FiR(P75)	Uncollimated epithermal neutron beam with 75-cm-long moderator at FiR 1
GBM	Glioblastoma multiforme
HFR	High Flux Reactor located in Petten, The Netherlands
IC	Ionisation chamber
ICRU	International Commission on Radiation Units and Measurements
INEEL	Idaho National Engineering and Environmental Laboratory
IRDF-90	International reactor dosimetry file cross section library
Kerma	Kinetic energy released per unit mass
K_n	Neutron kerma
$k_{B,tumour\text{-}to\text{-}blood}$	^{10}B concentration ratio of tumour-to-blood
$k_{B,brain\text{-}to\text{-}blood}$	^{10}B concentration ratio of normal brain-to-blood
LET	Linear energy transfer

Liquid A	Brain equivalent tissue substitute liquid without minor elements
Liquid B	Brain equivalent tissue substitute liquid with minor elements
MC	Monte Carlo
MCNP	A general Monte Carlo n-particle transport code
MITR-II	Massachusetts Institute of Technology Research Reactor located in Boston, USA
MR	Magnetic resonance
MU	Monitor units
$\dot{MU}_{Ref}$	Reference monitor unit rate
NCT	Neutron capture therapy
PET	Positron emission tomography
PMMA	Polymethylmethacrylate
PTV	Planning target volume
$r_{Au\text{-}197}$	^{197}Au(n,γ) activation reaction rate
$r_{Mn\text{-}55}$	^{55}Mn(n,γ) activation reaction rate
RBE	Relative biological effectiveness
rtt_MC	Radiation transport in tissue by Monte Carlo
SERA	Simulation environment for radiotherapy applications
TLD	Thermoluminescent detector
TORT	Three-dimensional discrete ordinates neutron/photon transport code
TPS	Treatment planning system
TS	Tissue substitute
VTT	Technical Research Centre of Finland
w-%	Percentage by mass
w_i	Experimental weighting factor of the absorbed dose D_i
1SD	One standard deviation
2D	Two-dimensional
3D	Three-dimensional

AIMS OF THE STUDY

The aim of this thesis was construction of the calculation model using the FiR 1 epithermal neutron beam for treatment planning in neutron capture therapy (NCT).

Specific aims of the study were as follows:

1) to create the FiR 1 epithermal neutron beam model and experimentally validate the free beam neutron spectrum (Study I)

2) to examine suitable brain tissue substitutes for NCT dosimetry (Study II)

3) to verify absorbed doses of the complete beam model in a phantom (Study III)

4) to transfer the beam model to a treatment planning system (TPS) and to validate and normalise the computed doses in TPS to measurements (Study IV)

5) to validate the dose planning chain of epithermal neutron irradiation without a boron carrier and to estimate uncertainties of computed dose components in NCT (Study V and Study VI)

6) to apply the FiR 1 beam model to BNCT treatment planning (Study VII)

1 INTRODUCTION

In 1899, four years after the discovery of X-rays, the first patient was reported to be cured using external radiation therapy [1]. Radiation therapy uses ionising radiation to treat patients with malignant tumours and selected benign diseases. The aim of radiotherapy is to deliver a accurate dose of irradiation in a defined tumour volume to destroy the tumour while causing minimal damage to surrounding healthy tissues [1]. In addition to X-rays, particles, such as electrons, neutrons, protons and light ions, have been used in external radiotherapy [2]. The rationale for the use of neutrons in preference to conventional X-rays is that neutron irradiation more effectively destroys radioresistant tumour cells [3]. The first clinical trials of fast neutron therapy started in 1938, six years after the discovery of neutrons by James Chadwick [4].

Like photons, neutrons have an influence indirectly through charged secondary particles. In conventional radiation therapy, megavoltage X-rays interact in tissue with atomic electrons mainly through the Compton effect and pair production [5]. Neutrons interact with atomic nuclei and induce nuclear particles, such as protons, α-particles and heavier nuclear recoils [6]. Neutron interactions include 1) capture in which the neutron is captured by a nucleus with emission of γ-radiation or with emission of proton irradiation (dominates at low energies), 2) elastic scattering, in which a recoil proton is produced in a collision of a neutron primarily with hydrogen nuclei and to a lesser degree with heavier atoms, 3) inelastic scattering, in which some of the energy is converted into γ-radiation or the nucleus is left in an excited state and 4) non-elastic interaction, in which nuclear reactions cause the emission of other particles [6].

Neutrons can be classified according to their kinetic energy as thermal (E<0.5 eV), epithermal (0.5 eV<E<10 keV) and fast (E>10 keV). The neutron dose D_n in tissue is equal to the neutron kerma K_n under the charge particle equilibrium [5],

$$D_n = K_n = \int_E f_n(E)\phi(E)dE, \quad (1)$$

where $f_n(E)$ is the neutron kerma factor (also called the fluence-to-kerma factor) for the interaction in matter, and $\phi(E)$ is the neutron fluence rate. The two most important interactions of thermal neutrons in tissue are the neutron capture by nitrogen $^{14}N(n,p)^{14}C^*$, and the neutron capture by hydrogen $^{1}H(n,\gamma)^{2}H$. In neutron capture therapy (NCT), the dose in tissue induced by the former reaction is called a nitrogen dose D_N, and by the latter a hydrogen capture gamma dose $D_{g,H}$. The kinetic energy of the proton from nitrogen capture is 0.58 MeV and proton range is approximately 10 μm in tissue. The kinetic energy of the hydrogen capture gamma ray is 2.2 MeV [5]. In addition to $D_{g,H}$, the minor contribution of the gamma dose from the other neutron capture reactions $D_{g,capture}$ in tissue elements (e.g. chlorine) is induced (Study II). From 40 eV to the higher neutron energies, the elastic scattering of neutrons with hydrogen nuclei $^{1}H(n,n')^{1}H$ begins to dominate the neutron kerma contribution in the brain tissue (Figure 1). In NCT, the dose component in tissue from this reaction is called the fast neutron dose D_{fast_n}. The contributions of oxygen-16 (^{16}O) and carbon-12 (^{12}C) are negligible (<1%) to the absorbed dose in tissue in the epithermal neutron beam with a low fast neutron dose contamination per epithermal neutron fluence rate ϕ_{epi} (D_{fast_n}/ϕ_{epi} = 2.1 x 10^{-13} Gycm^2). In addition to the neutron-induced doses in tissue, gamma rays in the incident neutron beam cause the so-called beam gamma dose $D_{g,beam}$. The beam gamma rays originate from the

materials in the reactor. $D_{g,beam}$ can cause up to 50% of the total gamma dose D_g in tissue in an epithermal neutron beam [7].

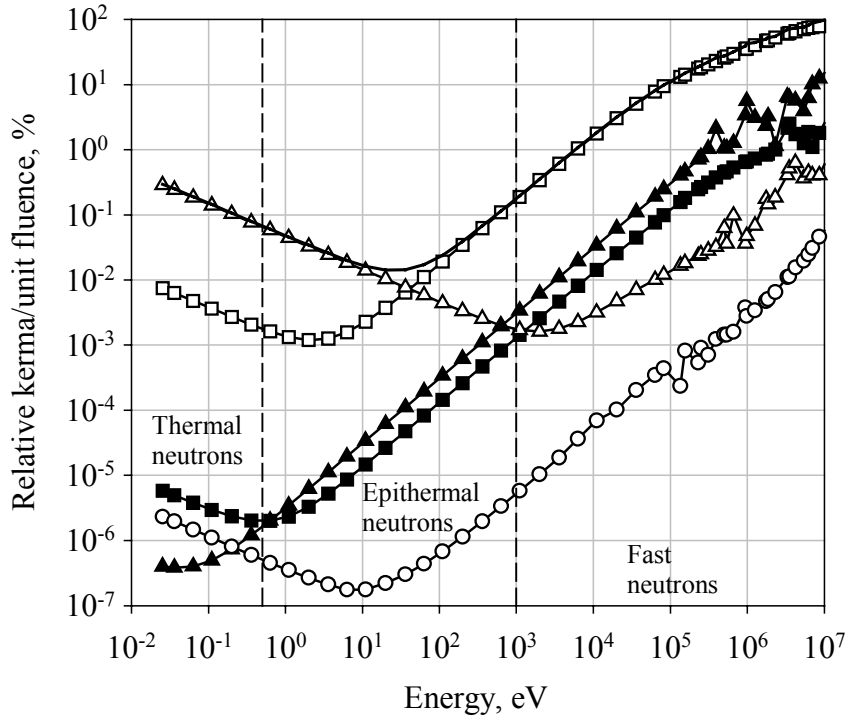

Figure 1. *Relative kerma per unit neutron fluence of the adult brain tissue (solid line) and of the five main atomic isotopes of the brain tissue [8, 9]: nitrogen-14 (open triangle), hydrogen-1 (open square), carbon-12 (solid square), phosphorus-31 (open circle) and oxygen-16 (solid triangle).*

The concept of NCT was first published by Locher in 1936 [10], who proposed the use of slow neutrons with strong neutron absorbers (e.g. boron, gadolinium) injected into tissue for selective destruction of cancerous tissues. To date, only boron has been used in NCT clinical trials of brain tumours, mostly glioblastoma multiforme (GBM), and melanoma [11-14]. Boron-10 (^{10}B) has a high cross section for the boron neutron capture reaction, ^{10}B(n,α)^{7}Li, at thermal neutron energies. The ranges of the high-LET α and ^{7}Li particles in tissue are approximately 9 and 5 μm, respectively, and the energies of the reaction are 2.3 MeV (94%) and 2.8 MeV (6%) [15]. The 0.48 MeV gamma ray is emitted in 94% of boron capture reactions, but the contribution to D_g is negligible. In boron NCT (BNCT), a boron delivery agent is injected into a patient's blood circulation, from where it accumulates in tumour cells, which are then externally irradiated with low-energy neutrons. If boronphenylalanine-fructose (BPA-F) is used as a delivery agent in BNCT of a GBM patient, the ^{10}B concentration in a viable tumour can be approximately four times more than in whole blood 0.5-1.5 hours after a 2-hour intravenous infusion, but it has considerable variation in the proportion of necrotic tissue [11, 16]. The ^{10}B concentration in a normal brain is slightly less than in blood [11]. When the dose from the boron neutron capture reaction (boron dose, D_B) is calculated in a tumour, the ^{10}B concentration ratio of tumour-to-blood $k_{B,tumour\text{-}to\text{-}blood}$ is assumed to be 3.5 and the ratio for the normal brain-to-blood $k_{B,brain\text{-}to\text{-}blood}$ 1.0 in order to calculate the dose in normal brain vascular endothelium [11]. If the ^{10}B concentration in blood $c_{B,blood}$ is assumed to

be 12 ppm on average during irradiation, D_B is approximately 75% of the total absorbed tumour dose at the dose maximum (Study VII).

From the 1950 up to 1994, only thermal neutron beams were used in BNCT. However, the dose distribution of the thermal neutrons was poor; the boron dose in tissue decreased to half in 2 cm [2]. To minimise the poor penetration of neutrons, the irradiation was given at the same time as craniotomy in Japan [2]. Epithermal neutrons were first utilised in USA in 1994 (MITR-II and BMRR) [15]. The epithermal neutrons thermalise in tissue and are captured by ^{10}B, causing D_B. The maximum D_B of the epithermal neutrons is approximately at a 2-cm depth in tissue and D_B reduces to half at 5-7 cm [17, 18]. The neutrons utilised so far in BNCT are produced by fission reactors in USA, Japan, the Netherlands, Finland, Sweden and the Czech Republic, but accelerator-based epithermal neutrons sources have also been under development [19-21].

In the recent decade, computational three-dimensional (3D) radiation treatment planning has increased significantly. Patient tomographic data are required to make an anatomical model of a target with planning target volume (PTV) [22] for the computation of 3D dose distribution. Transversal images are usually used [23]. In photon and electron therapy, CT images are utilised since they include information about the electron density of tissues. Thus, individual information about tissue contents is available to compute the dose distribution. For BNCT, several kinds of images are needed. With CT images, soft tissues, bones and air cavities, in which neutron transport differs, can be distinguished. However, CT data are inadequate to define the individual tissue compositions in BNCT since the images do not include atomic nuclear information. With MR images, by contrast, soft tissues and macroscopic tumour areas can be differentiated sufficiently well for the purposes of treatment planning. In the BNCT treatment plan, the information about boron distributions has been described as homogeneous inside the outlined tissues. The tissue-specific ^{10}B concentrations are based on the tissue-to-blood ratio of biological models [24]. However, the boron distribution in tissues is patient-specific and the treatment plan would be enhanced by including this information. The current BNCT treatment planning system (TPS) applies only one type of image at a time; however, future plans will include adding boron localisation data derived from PET images [25]. In the Finnish BNCT GBM research, MR images have been used in the TPS [26]. An anatomic few-region computational model of the patient's head with PTV and the tumour volume is delineated, and the tissue composition is defined according to ICRU 46 [8].

To produce the dose distributions in a patient model, a beam description for TPS is required [23]. The neutron capture therapy beams, generated at reactors, are individual beams with beam-specific properties [27]. Therefore, the model of the beam construction is generated using a neutron transport code. Specific methods have been utilised to solve the Boltzmann transport equation in the geometrical model. Two of the most commonly used modelling methods are the stochastic Monte Carlo method and the deterministic discrete ordinate method [28]. A general Monte Carlo n-particle transport code (MCNP) [29] is a typical Monte Carlo-based program for nuclear reactor simulations. The advantages of the MCNP are a continuous cross section library at all energies and the capability to model complex geometries. However, the statistical nature of the program requires extensive computer time to achieve a low statistical uncertainty and the solution is achieved only in specific tallies requested by the user [29]. The current TPSs used in BNCT are based on the Monte Carlo method [14, 30]. The discrete ordinate method produces direction-, space- and energy-dependent neutron and photon intensities at all points in the computational geometry [28]. The

advantage of the discrete ordinate method is that in only a few hours computing time the solution in the whole geometry is converged to a pre-set accuracy level. The discrete ordinate programs ANISN, DORT and TORT have been used in the design studies of an epithermal neutron beam [31-33]. The preliminary design of the Finnish epithermal neutron beam and the optimisation of a neutron moderator material were done with ANISN and TORT [31].

The neutron-photon beam model was created based on the reactor model. The beam model includes a description of the energy- and direction-dependent neutron and photon spectra. In addition, the geometrical structures starting from the neutron-photon spectra source plane to the beam entry are described in the beam model. The neutron spectrum of the beam can be verified experimentally free in air [34]. Prior to use in patient treatment planning, the beam model needs to be validated experimentally in a situation similar to the patient radiation treatment. The validation is done in phantom measurements. International recommendations for NCT dosimetry are still underway [35].

The computation of dose distributions for BNCT is a complex 3D problem since the dose components have different spatial distributions and biological responses [28]. In treatment planning, the distributions of dose components (D_g, D_B, D_N and D_{fast_n}) are computed in a geometric model of a patient's head (or body). Each dose component in tissue is weighted using experimental factors to get an approximate photon-equivalent dose that can be summed with the other dose components to get the total weighted dose D_W. The weighting factors of gamma (w_g), nitrogen (w_N) and fast neutron doses (w_{fast_n}) are equal for all tissues, but D_B has a tissue- and compound-specific weighting factor (w_B) [24]. D_W is a sum of the radiobiologically weighted dose components,

$$D_W = w_g D_g + w_B D_B + w_N D_N + w_{fast\_n} D_{fast\_n}, \tag{2}$$

and the absorbed dose components are:

$$\begin{cases} D_{\mathrm{g}} = D_{\mathrm{g,beam}} + D_{\mathrm{g,capture}} \\ D_{\mathrm{B}} = \mathrm{c}_{\mathrm{B,blood}} \mathrm{k}_{\mathrm{B,tissue\text{-}to\text{-}blood}} \int_E f_{B,ppm}(E)\phi(E)dE \\ D_N = \int_E f_N(E)\phi(E)dE \\ D_{fast\_n} = \int_E f_{fast\_n}(E)\phi(E)dE, \end{cases}$$

where $k_{B,tissue\text{-}to\text{-}blood}$ is the ^{10}B concentration ratio of tissue-to-blood, $f_{B,ppm}(E)$ is the ^{10}B kerma factor for 1 ppm ^{10}B concentration, $f_N(E)$ is the nitrogen kerma factor and $f_{fast\_n}(E)$ is the fast neutron kerma factor. Tables of kerma factors are published in literature, e.g. ICRU 46 [31].

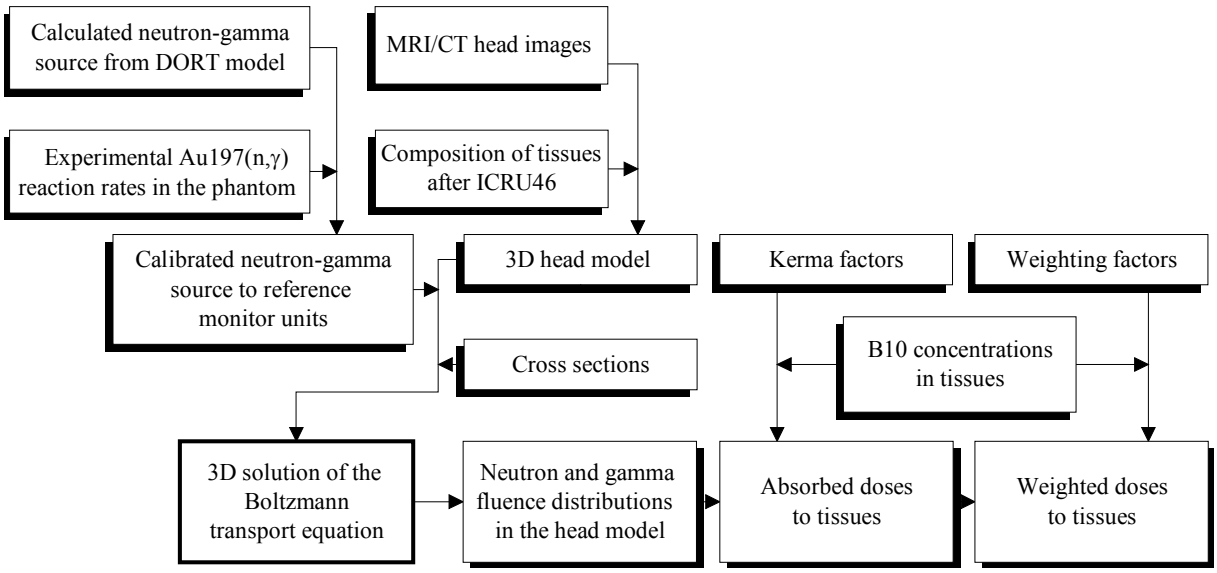

Figure 2. *Scheme of the BNCT dose calculation.*

The scheme of the dose calculation in the treatment planning system used in the Finnish BNCT (Study VII) is described in Figure 2. The elements that the user can influence in the dose calculation are neutron-gamma source, head model including tissue compositions, ^{10}B concentrations in tissues and weighting factors.

The BNCT doses are reported with isodoses and dose-volume histograms in normal brain tissue, in PTV and in tumour volume (Study VII). The tumour isodose distribution in BNCT with BPA-F is presented on a transaxial MR image of a GBM patient in Figure 3.

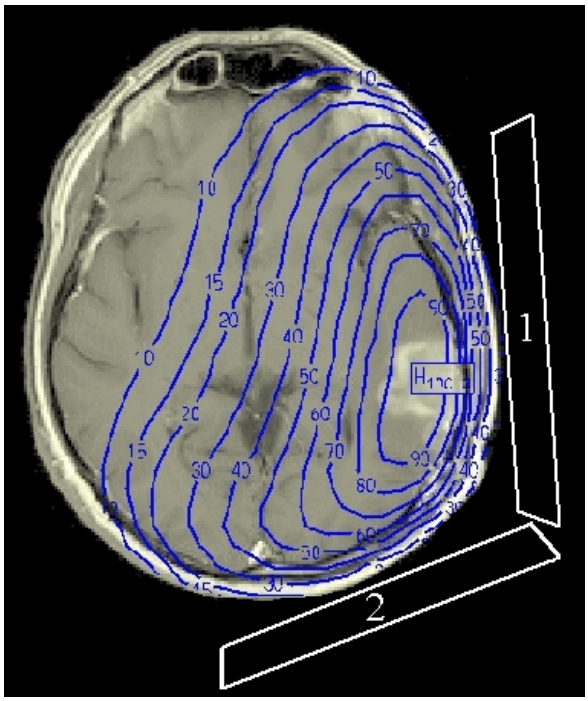

Figure 3. *Relative isodoses of the weighted total dose D_W for a tumour of a GBM patient, transaxial plane. The weights of the two fields are 0.6 (1) and 0.4 (2). Collimator edges are outlined.*

The horizontal cylindrical model of the FiR 1 epithermal neutron beam was created using DORT code [36] for computational dosimetry and BNCT treatment planning of brain tumours. The neutron collimator was designed using this DORT model. To experimentally validate the beam model, suitable brain tissue substitute (TS) phantom materials were simulated. The computed thermal neutron fluence and neutron dose and gamma dose distributions were verified with measurements in homogeneous phantoms consisting of three TS materials (PMMA, water and brain-equivalent liquid). The neutron-photon source from the DORT model was transferred to the treatment planning system. The experimental validation of the TPS with the FiR 1 beam model was done using the phantom measurements. The normalisation of the beam model to the measurements in a phantom was examined. The chain of the dose planning procedure was extensively studied in a healthy tissue tolerance study of the dog brain without the boron carrier. Finally, the TPS with the FiR 1 beam model was applied in the BNCT treatment planning of human glioma patients in the Finnish BNCT project.

In a previously published Ph.D. thesis in the Finnish BNCT project, the FiR 1 beam model was applied as part of the investigations of 1) the applicability of thermoluminescent dosimeters for BNCT [37], 2) the dose determinations in a phantom with twin ionisation chambers [38], 3) the relative biological effectiveness of the beam for the canine brain [39] and 4) the experimental dosimetry system and patient positioning [40].

2 MODELLING OF THE FIR 1 EPITHERMAL NEUTRON BEAM

The epithermal neutron beam is generated at the Finnish research reactor (FiR 1), which is a 250 kW TRIGA Mark-II type of open pool light water-cooled and graphite-reflected nuclear reactor (General Atomics Company, USA). The fuel elements in the reactor core are asymmetrically loaded so that the fresh fuel rods are in the direction of the epithermal beam to maximise beam intensity. The final configuration of the epithermal neutron beam FiR(K63) is moderated with a 63 cm FLUENTAL™ moderator [31] and collimated by a bismuth (Bi) cone [27]. FLUENTAL™ (69 w-% AlF_3, 30 w-% Al and 1 w-% LiF, density 3 g/cm^3) is a neutron moderator material that was developed at VTT [31]. Mainly because of the FLUENTAL™ moderator, a high-intensity, collimated epithermal neutron beam with low fast neutron and gamma ray contamination has been achieved at the low power research reactor. The FiR(K63) beam, completed in November 1997, was the first epithermal neutron beam with all these characteristics to be utilised in BNCT.

A two-dimensional (2D) horizontal cylindrical model of the FiR 1 epithermal beam was constructed with a DORT code [36] with a BUGLE-80 [41] coupled (47 neutron and 20 photon groups) cross section library. A forward-biased quadrature set (D_{166}) was selected for the collimated beam model (Study I). Three geometries of the beam in its different stages were modelled, i.e. FiR(P75), FiR(K75), FiR(K63), and validated experimentally [17, 34, 42-44]. FiR(P75) had a 75-cm-thick FLUENTAL™ moderator and was uncollimated. FiR(K75) also had a 75 cm moderator and was collimated. The DORT models have been used in the optimisation of the final thickness of the moderator [31], in the design of the beam collimator and in the shielding of the facility [45]. In addition to the design computations, the DORT models of the beam have been used in computational dosimetry and BNCT treatment planning (Studies I-VII). For the most part, the clinically used FiR(K63) beam model is discussed in detail in this thesis. The FiR(K63) beam has a 63-cm-thick FLUENTAL™ moderator and is collimated.

The DORT model of the beam consists of a description from the reactor core to the beam exit with a surrounding geometry (Study I). The model was divided into two parts, core and moderator-collimator. The core model was a fission neutron source that was tailored to a collimated epithermal neutron beam with the beam moderators and the collimator in the second part of the model. The principle of changing the real 3D geometry, where the reactor core is vertical cylindrical, to the horizontal cylindrical model was that the distances of the structures in the epithermal neutron beam central line were real. The central line of the cylinder model was the middle line of the core, the FLUENTAL™ moderator and the collimator. The rectangle structures of the real geometry were adjusted in the radial direction of the cylindrical model so that the volumes of the structures remained of equal size. This solution with DORT code and BUGLE-80 library has been used earlier in the design and evaluation of other epithermal neutron beams facilities for BNCT [32, 33, 46]. The FiR 1 graphite reflector with an air-filled irradiation ring around the active core and a tangential air tube between the active core and the moderators were modelled so that the graphite densities were reduced to correspond the averaged densities of the modelled areas in the direction of the beam. Initially, the FiR 1 core was modelled to be homogeneous and no air-filled structures (tangential tube and irradiation ring) in the area of the graphite reflector were taken into account. The first measurements showed a 50% underestimation in the beam intensity of the initial model [42], therefore, a more detailed model of the core was constructed. The most

essential details of the core model and the collimator design are explained in sections 2.1 and 2.2.

2.1 Core as neutron source

The core model includes the active reactor core, the graphite reflector with the irradiation ring and the tangential tube, part of the moderating water and the initial part of the epithermal column with aluminium frame, a boral plate (thermal neutron absorber) and part of the neutron moderator. The atom densities of the fuel rods are based on the burn-up of the rods (Study I).

The vertically cylindrical reactor core contains 79 three-types of fuel rods with zirconiumhydrid, four B_4C control rods, four graphite rods and four other rods surrounded by light water. The fuel rods consist of twenty-three 12 w-% uranium (U) rods (steel shell), seven 8.5 w-% U rods (steel shell) and forty-nine 8 w-% U rods (Al shell). The uranium-235 (^{235}U) enrichment is 20 w-% [47]. The fuel rods in the reactor core are loaded asymmetrically so that the freshest fuel rods are loaded in the direction of the beam (Figure 4). The initial MCNP computation showed that the oblique fuel loading increases the neutron intensity in the beam direction by 30% as compared with basic fuel loading, where the freshest fuel rods are in the middle rings of the core [47].

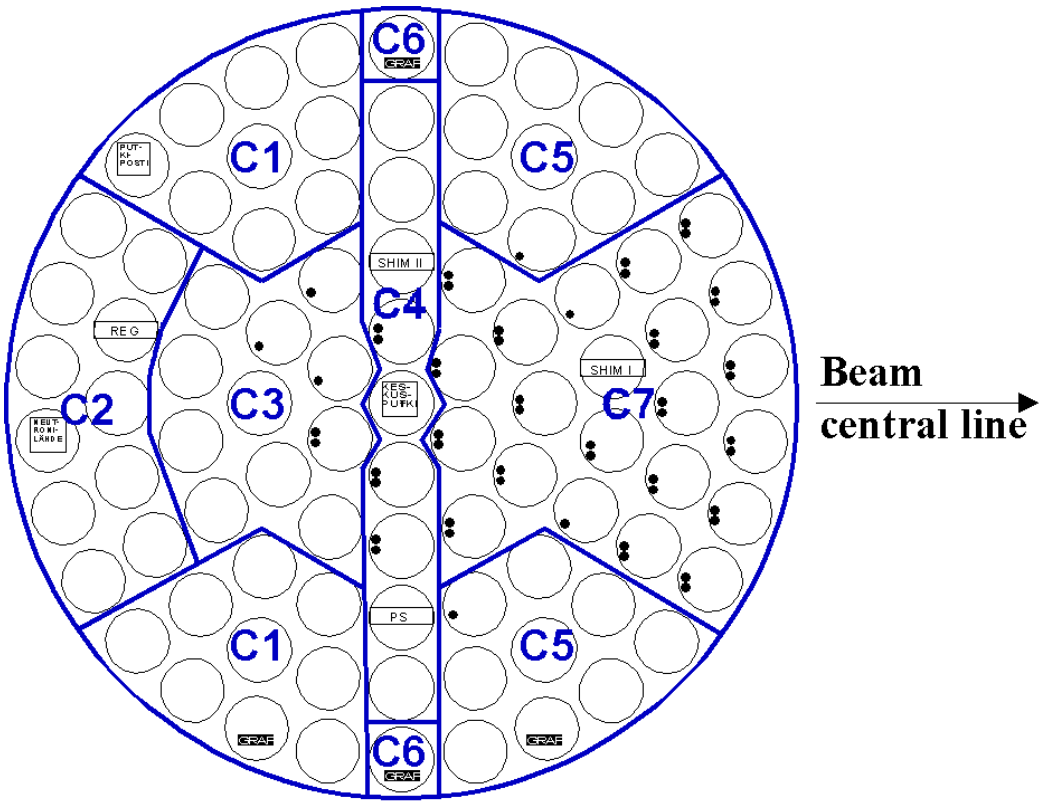

Figure 4. *Core loading of the FiR 1 reactor and active core zones (C1-C7) of the DORT core model. The 79 fuel rods consist of 12% U (two dots), 8.5% U (one dot) and 8% U rods that are asymmetrically loaded.*

The asymmetrical core rod loading was taken into account in the DORT model. The rods in the core model were divided into the seven zones (Figure 4). The basic idea to divide the rods into these zones C1-C7 was that the same types of rods be in the same zone and that distant rods from the beam central line be put into separate zones (C1, C5). The water around the rods was included in the core zones. The fuel rods with the highest ^{235}U concentration were in zone C7. The ^{235}U contents of the individual fuel elements compared with fresh 12 w-% U fuel rods were 52-57% (C1), 53-57% (C2), 52-94% (C3), 54-93% (C4), 54-57% (C5), and 56-100% (C7). Zone C6 did not include fuel elements. The percentage sizes and ^{235}U atom densities of the core zones (C1-C7) in the heterogeneous core model compared with the initial homogenised core zone are shown in Table 1.

Table 1. *Percentage sizes and ^{235}U atom densities of the core zones (C1-C7) in the heterogeneous core model as compared with the average ^{235}U atom densities in the homogenised core model. Atom density of ^{235}U in the homogenised core zone was 1.41 x 10^{20} atoms/cm^3.*

	C1	C2	C3	C4	C5	C6	C7
Size, %	20	11	12	9	20	2	26
U^{235}, %	81	79	97	91	83	0	150

Two control rods (B_4C) were in zones C2 and C4. Two other control rods in zones C4 and C7 are up (not in use) when the reactor is running so they were included in the model as water. Zone C6 consisted of only two graphite rods, and the two other graphite rods were in zones C1 and C5. One (central rod) of the four other rods is filled with water and two with air, and one (neutron source) is entirely water without a shell.

Around the reactor core is a graphite reflector ring which reflects escaping neutrons to the core to take part in the fission reactions (Study I). The air-filled tangential tube, between the core and the moderators, and the air-filled irradiation ring around the core were included in the heterogeneous core model. The air volumes in the tube and the ring were included in the core model by reducing the graphite densities. The graphite reflector in the beam direction was divided into four graphite zones (Study I). A thin graphite layer (C) between the core and the tangential tube was 100% graphite to achieve a full reflection of fission neutrons back to the reactor core. The reduced densities of the three graphite reflector zones due to the tangential tube and irradiation ring were calculated in the direction of the epithermal neutron beam and used in the model. The graphite densities of the zones were 44.6%, 51.4% and 64.3% from the central axis to outwards in the radial direction. In Study I Figure 2a, the graphite density of the middle zone was misprinted.

When converting the homogeneous core model to heterogeneous ones (C1-C7), the thermal neutron fluence rate ϕ_{th} increased in a phantom at the beam exit by a factor of 1.35. This result was in agreement with the initial MCNP simulation [47]. The reduction of graphite densities (use of real densities) between the core and the moderator increased beam intensity by 15%. Thus, when the heterogeneous core model was used and the optic densities of graphite reflector were taken into account, the beam intensity increased 50% and was in agreement with initial measurements in the FiR(P75) beam geometry [42].

2.2 Beam tailoring with moderator and collimator

In the second part of the DORT model, the fission neutrons were moderated to the collimated epithermal neutrons (Study I). The purpose of these geometrical structures is to achieve a high-intensity, well-collimated epithermal neutron beam that has a very low fast neutron and photon contamination in the beam. In the first stage (1996) of the collimated beam, FiR(K75), the moderator thickness was 75 cm. The dosimetric measurements revealed that the fast neutron contamination in the beam was very low ($D_{fast\_n}/\phi_{epi} = 1.0 \times 10^{-13}$ Gycm^{2}s) but that the beam intensity ($\phi_{epi} = 0.5 \times 10^9$ n/cm^{2}s) should be increased [42, 43]. The DORT computations predicted that shortening the moderator from 75 cm to 63 cm would increase the intensity of ϕ_{th} in a phantom, to which D_B is directly proportional, at the thermal neutron maximum by a factor of 2.0 and at 50% of the thermal neutron maximum by 2.04. D_{fast_n}/ϕ_{th} in a phantom, which describes the quality of the epithermal neutron beam, increased at the thermal neutron maximum by a factor of 2.2. The moderator was shortened to 63 cm and the measurements confirmed that the free beam epithermal neutrons, which thermalise in a phantom, doubled their intensity (Study I).

The conical Bi collimator with lithium-polyethylene shielding was designed with the FiR(K75) model. A well-collimated epithermal neutron beam increases the desired thermal neutron fluence (and the boron dose) at the depth in tissue per entrance neutron dose [32]. The effects of collimator length on BNCT doses in a head-size PMMA phantom and on beam forwardness (current-to-flux ratio) at the free beam exit were examined using a circular 14-cm-diameter beam. The Bi collimator lengths were 25, 47 and 103 cm, with corresponding cone angles of 96°, 62° and 31°. The Bi collimator thickness was fixed to 7 cm. In Table 2, the effects of collimator length on BNCT doses relative to the doses of the 103-cm collimator and the free beam current-to-flux ratios for each collimator length are presented. The planned minimum current-to-flux ratio of 0.75 was achieved with the 47-cm-long collimator (Table 2). Using the 25-cm-long collimator, D_B was almost five times higher than using the 103-cm-long collimator, the latter of which would provide a very good current-to-flux ratio (0.85). The undesirable D_{fast_n} at the surface can be decreased with the more collimated beam, i.e. with a higher current-to-flux ratio, as a previous study suggests [32].

Table 2. *Effect of collimator length on BNCT doses in a phantom. D_B, D_N, D_g and D_{fast_n} are presented relative to those of a 103-cm collimator. Current-to-flux ratios at the free beam exit are for each collimator length.*

Length, cm	D_B and D_N at 2.5-cm depth	D_g at 2.5-cm depth	D_{fast_n} at 0-cm depth	Current-to-flux at free beam exit
25	4.69	4.74	5.84	0.67
47	3.16	3.20	3.47	0.75
103	1.00	1.00	1.00	0.85

The highly collimated beam reduced beam intensity significantly (Table 2). Intensity can be improved with the thicker Bi collimator, which reflects neutrons back to the beam. In Table 3, the effects of collimator thickness (0, 7 and 10 cm) on BNCT doses in the phantom with a 47-cm-long Bi collimator are presented. The comparison revealed that the 7-cm- and 10-cm-thick Bi collimators increased D_B by 43% and 57%, respectively, compared with the bare conical

lithiated polyethylene collimator with no Bi layer. The avoided D_{fast_n} at the surface of the phantom increased more than the desired D_B in the phantom with the Bi layer.

Table 3. *Effect of collimator thickness on D_B, D_N, D_g and D_{fast_n} in a phantom. The dose componets are presented relative to those of the collimator with no Bi layer.*

Thickness, cm	D_B and D_N at 2.5-cm depth	D_g at 2.5-cm depth	D_{fast_n} at 0-cm depth
10	1.57	1.53	1.73
7	1.43	1.40	1.58
0	1.00	1.00	1.00

As a compromise between the intensity and collimation of the beam, the 46.6-cm-long collimator with a 60° angle was constructed [27]. A 7-cm-thick Bi collimator (approximately 500 kg) was chosen. The 10-cm-thick Bi collimator layer would increase beam intensity by 10% compared with the 7-cm Bi collimator, but the weight of the Bi collimator would rise to 750 kg. The final current-to-flux ratio was calculated to be 0.77 at the exit plane of the 14-cm aperture.

2.3 Experimental validation of free beam spectrum

The FiR(K63) free beam neutron spectrum at the beam entry was measured as described in Study I. Comparisons of the calculated and the experimental thermal (E<0.5 eV), epithermal (0.5 eV<E<10 keV) and fast (E>10 keV) neutron fluence rates are presented in Table 4. The experimental values are the most recent and have changed slightly from the values in Study I because of small modifications to the adjustment data (e.g. tungsten decay data).

Table 4. *Calculated (C) and experimental (E) (± 1SD) neutron fluence rates ϕ at the beam exit plane of the 14-cm aperture.*

	ϕ, n/cm^{2}s		Ratio
	C	E	C/E
Fast Neutrons	3.20×10^7	3.45×10^7 (±31%)	0.93
Epithermal Neutrons	1.03×10^9	1.07×10^9 (±5%)	0.96
Thermal Neutrons	6.65×10^7	7.19×10^7 (±21%)	0.92

Previous DORT computations with BUGLE-80 cross sections of the epithermal neutron beam with an aluminium-oxygen neutron moderator underestimated the fast neutron component by 30-50% [32, 33, 46]. As suggested by Nigg *et al*. [46], the problem is not as severe with an aluminium-fluorine moderator. Experimental validation of the free beam spectrum showed that the calculations and the measurements of energy groups were in good agreement (Table 4). Comparative measurements of the INEEL dosimetric group (Idaho Falls, USA) confirmed the good agreement of experimental and computational fluence rates [48].

3 VERIFICATION OF BEAM MODEL IN PHANTOMS

The FiR(K63) epithermal neutron beam has five fixed sizes of circular fields for irradiation. The available diameters of the beam are 8, 11, 14, 17 and 20 cm. The 11-cm and 14-cm-diameter beams were selected for use in the BNCT of brain tumour patients. It was decided that in BNCT a patient‘s head should be next to the beam aperture since the beam is somewhat diverging, and if a patient is moved further away, treatment times become longer and the dose to healthy tissues increases with aperture size. Therefore, a phantom that is used for dosimetric validation of the beam model is also placed next to the beam exit plane.

Generally, a beam in BNCT has been characterised in a TS phantom by measuring the thermal neutron fluence Φ_{th}, gamma dose D_g and fast neutron dose D_{fast_n} in the central axis of a phantom under reference conditions [18, 49]. With the exception of D_{fast_n} and the beam gamma dose $D_{g,beam}$, all significant dose components in BNCT are induced from Φ_{th} generated in the irradiation volume [32]. Because the fast neutron and gamma ray contaminations in the FiR(K63) beam are very low (D_{fast_n}/ϕ_{epi} = 2.1 x 10^{-13} Gycm^{2}s, D_g/ϕ_{epi} = 0.5 x 10^{-13} Gycm^{2}s) [27, 50], characterisation of ϕ_{th} in a phantom is especially important. However, experimental validation of the computed gamma and neutron doses in phantoms assures that the fast neutrons and gamma rays in the beam are correctly modelled. In addition, validating that the thermal neutron-induced doses in a phantom and in tissue are correctly computed in a TPS is important.

3.1 Tissue substitute phantom materials

Prior to the dose planning in tissue, the computations were validated with dosimetric measurements in TS phantoms. In photon and fast neutron therapy, water is used as a reference phantom material [51]. The TS phantoms are used for experimental validation of a beam model, dose calibration and quality control. TS phantoms are also used in dosimetric intercomparison of epithermal neutron beams, which is underway in the European Code of Practice project [35]. In NCT dosimetry, no commonly accepted recommendations for TS phantoms exist, therefore, a suitable TS material was studied (Study II). In previous experimental NCT dosimetric studies [49, 52, 53], both water and PMMA (polymethylmethacrylate) were used as phantom material. Both materials have shortcomings compared with adult brain tissue content as defined by ICRU 46 [8] in their elemental compositions. For example, nitrogen and minor elements (P, Na, Cl, K, S) are absent in water and in PMMA. In addition, the hydrogen atomic density is 15% lower in PMMA and 1.5% higher in water than in brain tissue [8]. As a consequence of these shortcomings, two new brain TS liquids were designed from chemical compounds (Study II). Both brain TS liquids (Liquids A and B) contained equal atomic densities to adult brain tissue of the main elements (H, O, C, N) [8]. Moreover, Liquid B included an equal amount of minor elements as in brain tissue [8]. The dose components in Liquid B were more similar than those in Liquid A to the ones in brain tissue, therefore Liquid A was excluded from future studies.

The computational comparison of neutron and photon transport calculations in these four brain TS candidates and in brain tissue predicted that D_g was 24-28% lower in PMMA than in brain tissue at the thermal neutron maximum (Study II). This variation is explained by differences in the neutron beam spectrum and gamma ray contamination in the beam. Both beams were uncollimated and one was the FiR(P75) beam with a simple delimiter (Beam 1 in Study II). The thermal neutron maximum was at 1.5-cm depth in the uncollimated beams. The

D_g was 10-12% lower in water than in brain tissue [8] at a depth of 1.5 cm. Water simulated Φ_{th} in the brain tissue 2 percentage units closer than PMMA at the thermal neutron maximum. In all tissues, fluence-to-kerma conversions to brain tissue were computed only to study the effect of neutron and photon transport calculations.

The TS phantom study (Study II) was repeated using the SERA treatment planning system (INEEL/MSU, USA) [25] with the collimated FiR(K63) epithermal neutron beam in the cylindrical phantoms (diameter 20 cm, length 24 cm) (Figure 5). The liquids were covered with a 0.5 cm PMMA frame. The thermal neutron maximum in the phantoms shifted to a depth of 2.0 cm in the collimated beam. In this set-up, the computed D_g was 21% lower in PMMA, 9% lower in water and 2% lower in Liquid B than in brain tissue at a depth of 2.0 cm. The computed Φ_{th} was 3% higher in PMMA, 6% higher in water and 0.2% lower in Liquid B than in the brain tissue (Figure 5). In the collimated beam, PMMA simulated Φ_{th} in the brain tissue at the thermal neutron maximum 3 percentage units closer than water. This is contrary to the observation in the uncollimated beam (Study II). The brain tissue-equivalent liquid (Liquid B) simulated excellently Φ_{th} and D_g in the brain tissue both in the collimated and the uncollimated beams.

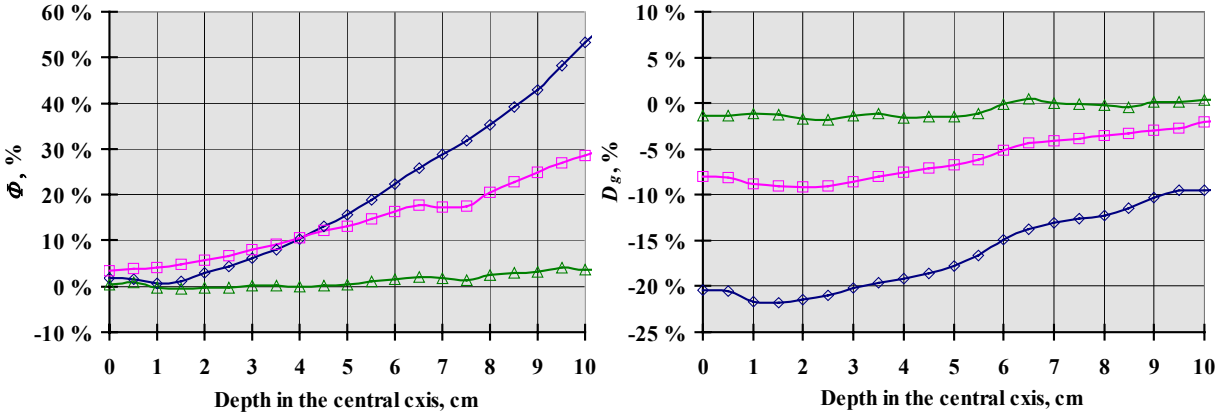

Figure 5. *Percentage difference of the thermal neutron fluence Φ_{th} (left) and the gamma dose D_g (right) in PMMA (diamond), water (square) and Liquid B (triangle) phantoms compared with the corresponding values in adult brain tissue [8] in the central axis of the cylindrical phantom in the collimated 14-cm-diameter FiR(K63) beam.*

Raaijmarkes *et al.* [54] studied the influence of composition of the phantom material in the high flux reactor (HFR) well-collimated epithermal neutron beam. In their beam, the thermal neutron maximum was at a depth of 2.0 cm in a tissue-equivalent (TE) phantom. Φ_{th} in a PMMA phantom was 1% lower, D_g 12% lower and D_{fast_n} 3% lower than in the water phantom. This is consistent with the phantom computations in the FiR(K63) beam. Small differences are explained with differences in neutron spectra and uncertainties in fluences/doses.

The PMMA, water and Liquid B phantoms were manufactured for the dosimetric measurements at the FiR 1 facility. Kortesniemi *et al.* [44] measured the gamma depth doses in the 14-cm FiR(K63) beam. The measurements showed that D_g was 10% lower in water and 20% lower in PMMA than in Liquid B at a depth of 2.0 cm of the cylindrical phantoms. These D_g differences agreed well with the SERA computations explained above. The activation foil measurements showed that Φ_{th} was 10% higher in water and 6% higher in PMMA than in Liquid B at a depth of 2.0 cm (Study IV). Uncertainty of the measured Φ_{th} was estimated to be

4% (1SD) [44]. Measurement showed differences a few percentages higher in Φ_{th} of phantoms than the computations had predicted, but these were still within the measurement uncertainties. According to both computations and measurements, Φ_{th} was 3-4% higher in water than in PMMA.

In conclusion, at the thermal neutron maximum, PMMA simulates Φ_{th} in brain tissue slightly better (3 percentage units closer) than water, but water simulates D_g in brain tissue better (12 percentage units closer) than PMMA in the collimated FiR(K63) beam. From the perspective of measurements, the PMMA phantom was more practical to use than the water phantom. The spatial accuracy of the detectors in solid material is superior to that in liquid. In addition, in liquids the detectors needed to be fixed to a measurement position with solid support materials, which might disturb the fluence/dose distributions of a homogeneous phantom material. Even though the brain-equivalent liquid (Liquid B) simulates the fluence/dose distributions in brain tissue well, the uncertainty of its composition was greater than that of water. Following advances in water, PMMA and Liquid B, all of these materials have been used in the experimental validation of the FiR 1 beam model and the computations in a phantom. Of these materials, PMMA was chosen for the normalisation of the beam model to activation measurements. The normalisation beam model is discussed in more detail in section 4.3.

3.2 Experimental verification

At least four activation foil/wire measurement techniques in a phantom have been used in epithermal neutron dosimetry at the clinical BNCT facilities. Liu *et al*. [52] at BMRR and Rogus *et al.* [49] at MITR-II have applied gold foils using the cadmium difference technique [5]. Raaijmarkers *et al*. [53] have also studied the two-foil method at HFR and have chosen this method in clinical NCT dosimetry with gold-aluminium (Au-Al) (5 w-% Au) and manganese-nickel (Mn-Ni) (88 w-% Mn) foils [18]. In intercomparative phantom measurements at FiR 1, Nigg *et al*. [17] used copper-gold wires with computed effective cross sections for flux wire materials.

In Finnish dosimetric measurements, diluted Au-Al (1 w-% Au) foils have been applied to determine ϕ_{th} in a phantom. Neutron spectra were computed in 47 BUGLE-80 energy groups using the DORT model at the measurement locations of a phantom. The ^{197}Au(n,γ) activation reaction rates $r_{Au\text{-}197}$ were calculated by multiplying the computed neutron fluence rates and the corresponding spectrum-weighted activation cross sections in energy groups. The weighting spectrum at a depth of 2.5 cm in a phantom was used to condense the 640-group activation cross section data from the IRDF-90 library [55] to the 47 BUGLE-80 neutron groups. The method is described in Study III more precisely. The measured Φ_{th} was determined by scaling the computed Φ_{th} by the ratio of the measured and the calculated ^{197}Au(n,γ) activation reaction rates at the measurement location. The uncertainty of the measured Φ_{th} in a phantom was estimated to be 4% (1SD) [44]. All the measured values used for the validation of computed values are reported at the reference monitor unit rate (reactor power approximately 250 kW). The calculated neutron fluence rate ϕ was normalised to the reference monitor unit rate $\dot{M}U_{\mathrm{Re}f}$ [56] by the ratio of the measured and the calculated ^{197}Au(n,γ) activation reaction rates at the thermal neutron maximum of the PMMA phantom (diameter 20 cm, depth 24 cm) (Study IV). A value of 0.95 for the ratio was determined for the circular 11-cm- and 14-cm-diameter beam models of the FiR(K63) DORT model.

The analysing method described above of the measured ϕ_{th} at the FiR 1 is dependent on the calculated DORT spectrum. It is practical method since only one measurement and one foil type are needed. However, the method is dependent on the computations and it assumes that the shape of the calculated neutron spectrum is correct. The validation of the neutron fluence can be done independently when the activation reaction rates are compared. The method becomes more reliable when two different energy-dependent foils are used; thus, diluted Mn-Al (1 w-% Mn) foils were also applied. In Figure 6, the computed proportional responses of the epithermal (0.414 eV<E<10 keV) and the thermal (E<0.414 eV) neutrons for the ^{197}Au(n,γ) and ^{55}Mn(n,γ) activation reaction rates $r_{Au\text{-}197}$ and $r_{Mn\text{-}55}$ at depths in the PMMA phantom of the 14-cm FiR(K63) beam are shown. At a depth of 2.0 cm, 58% of $r_{Au\text{-}197}$ and 97% of $r_{Mn\text{-}55}$ originate from the thermal neutrons, and the remainder is induced from the epithermal neutrons. The fast neutron's response (E>10 keV) for both activation reactions was negligible (<0.01%).

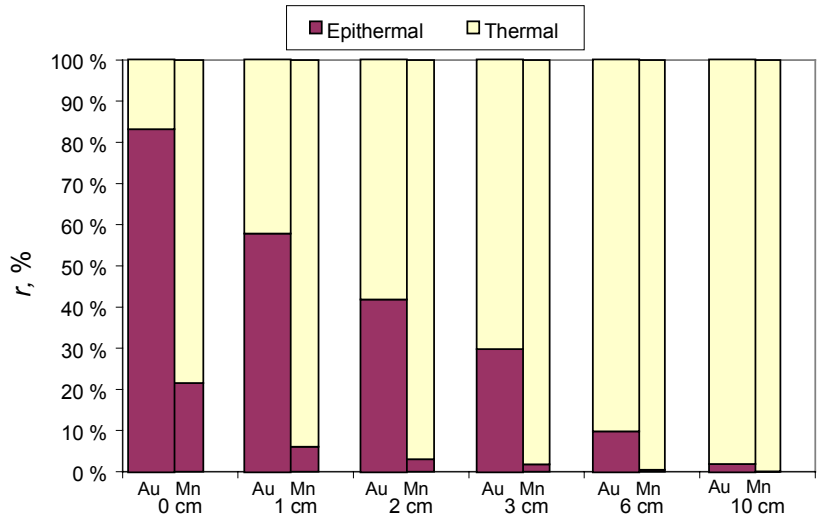

Figure 6. *Proportional responses of the epithermal (0.414 eV<E<10 keV) and thermal (E<0.414 eV) neutrons for the ^{197}Au(n,γ) and ^{55}Mn(n,γ) activation reaction rates r in the central axis of the cylindrical PMMA phantom in the 14-cm FiR(K63) beam.*

The DORT model of the FiR(K63) beam was verified with the Au and Mn activation reaction rate measurements in the cylindrical (diameter 20 cm, length 24 cm) PMMA, water and brain-equivalent liquid (Liquid B) phantoms (liquid phantoms were attached to the pool [44]). The Mn foils were only used in the PMMA phantom that best simulates Φ_{th} in the brain tissue and has the lowest uncertainty of the detector position. The uncertainty of the measured activation reaction rate is estimated to be 3% (1SD). The verification of the model with a circular 14-cm-diameter beam is presented in the central axis and in the selected off-axis points (depths of 2.5 cm and 6.0 cm) of the phantoms (Figure 7). The results of the comparison were similar to the 11-cm-diameter beam.

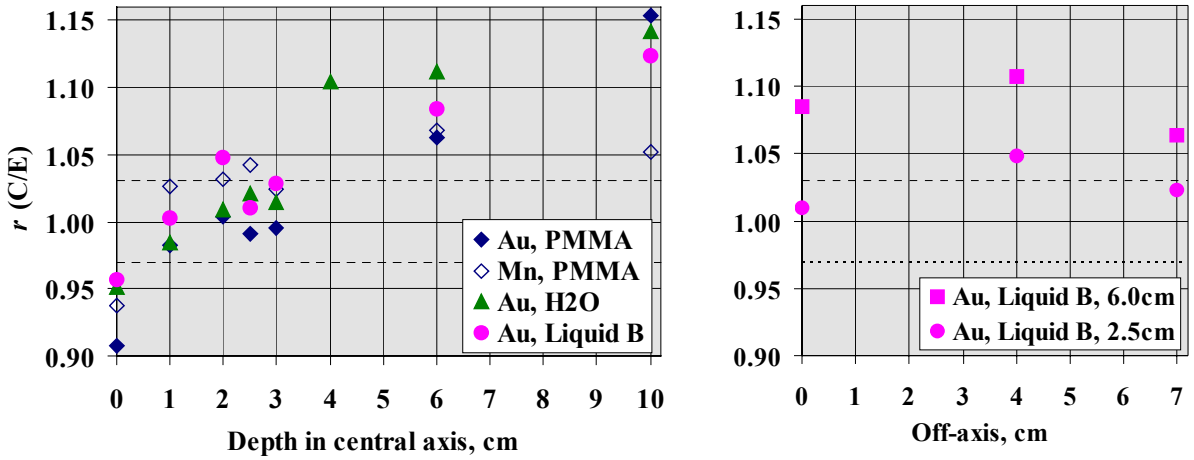

Figure 7. *Ratio of calculated (DORT) and experimental (C/E) $^{197}Au(n,\gamma)$ and $^{55}Mn(n,\gamma)$ activation reaction rates r in three cylindrical phantoms in the 14-cm beam. The dotted lines describe the measurement uncertainty of 3% (1SD).*

The comparison showed (Figure 7) that near the thermal neutron maximum at a depth of 2.0 cm most of the C/E ratios were within the measurement uncertainty of 3% (1SD). At the beam entry, the calculated reaction rates were systemically underestimated by about 5%. At deeper depths in the phantom, the calculated reaction rates were overestimated by up to 16%. An explanation for the ascending C/E ratios as a function of depth in Figure 7 is that only a single weighting spectrum (at 2.5-cm depth) was used for the regrouping of the activation cross sections for all depths and the BUGLE-80 library consists of only two thermal neutron energy groups. The similar C/E ratios of $r_{Au\text{-}197}$ and $r_{Mn\text{-}55}$ in the PMMA phantom predict that the computed neutron spectra at the epithermal and thermal neutron energy areas were approximately correct.

Water was observed to simulate the gamma dose D_g in the brain tissue considerably closer (more than 10%) than PMMA in three different epithermal neutron beams (Figure 5 and Study II). Thus, water was primarily used in the experimental validation of the absorbed gamma dose. According to the computations in the 14-cm FiR(K63) beam, approximately 95% of the gamma dose at the thermal neutron maximum in the water phantom originated from the hydrogen capture reaction, $^{1}H(n,\gamma)^{2}H$, and only 5% of the beam gamma rays. Therefore, the uncertainty of the computed hydrogen capture gamma dose $D_{g,H}$ is highly dependent on the uncertainty of the computed Φ_{th}. The calculated and the measured Φ_{th} in the neighbourhood of its maximum in the 14-cm beam were within 2.5%, the uncertainty of the measured Φ_{th} is 4% (1SD) and the uncertainty of the used mass energy absorption coefficient is 1% for hydrogen [8]. When considering these uncertainties, the combined quadratic uncertainty of the calculated $D_{g,H}$ around the thermal neutron maximum was estimated to be 5% in the water phantom.

The calculated total neutron and gamma doses D_n and D_g to the brain tissue defined by ICRU 46 [8] were validated using twin ionisation chamber measurements in the phantoms (Study III). The computed neutron spectra of the DORT model at the measurement locations in the water phantom were used to determine the experimental neutron doses D_n. According to this study, the uncertainties (1SD) of the measured D_n and D_g were estimated to be 6.3% and 21.5%, respectively. The comparison of the calculated (DORT) and the measured (ionisation chambers, Exradin) gamma doses at the thermal neutron maximum showed that the calculated

gamma dose was 5% higher than the measured gamma dose. In these computations, the beam intensity adjustment was -3.6% based on the Au-Al activation foil normalisation (Study III). However, additional Au-Al activation measurements (n=6) in the PMMA phantom increased the beam intensity adjustment of the DORT model from -3.6% to -5.0%. After this new intensity adjustment, the renormalised calculated gamma dose was only 3.5% higher than the measured gamma dose at the thermal neutron maximum. To make the comparison more reliable, the measurements should be extended to the surface direction in a phantom. In the horizontal beam, this would be technically cumbersome because of the solid frame around the water phantom and the large size of the IC detector. However, the comparison of the measurements and calculation of absorbed gamma dose in the water phantom suggest that the photons in the beam were modelled correctly within the IC measurement uncertainty of 6.3%.

In NCT, the total neutron dose D_n in tissue consists mainly of the nitrogen dose and the fast neutron dose. The main part of D_n in the FiR(K63) beam is from the nitrogen capture since the fast neutron contamination is very low [50]. The measured (pair ionisation chamber, Exradin) and the calculated total neutron doses agreed well in the water phantom within the measurement uncertainty of 21.5% (Study III). At the first measurement depth (2.0 cm), the calculated D_{fast_n} dose was about 20% of the total neutron dose D_n. Since the amount of the fast neutron dose of the total neutron dose and the measurement uncertainty are approximately equal (~20%), the uncertainty of the calculated fast neutron dose D_{fast_n} remains large. At the surface of the phantom, the calculated D_{fast_n} was 73% of the total neutron dose D_n; however, comparison to the experimental IC data could not be made because of difficulties due to the horizontal beam explained above. The experimental fast neutron fluence rate free in air agreed well within the measurement uncertainty of 31% (Table 4). The uncertainty of the kerma factors for hydrogen is 1% [8]. Therefore, the uncertainty of the calculated D_{fast_n} in a phantom was estimated to be 31%.

4 TRANSFERRING BEAM MODEL FOR TREATMENT PLANNING SYSTEM

The BNCT treatment planning has been performed with the Monte Carlo based 3D computational treatment planning systems (TPSs) [14, 30]. In the Finnish BNCT project, the BNCT_Rtpe software (INEEL/MSU, USA) was initially used in NCT and BNCT dose planning. Its successor SERA (INEEL/MSU, USA) was later taken into use at FiR 1. The main difference between the programs is that SERA uses approximately ten times less computer time than BNCT_Rtpe. One field dose computation in SERA takes less than half an hour depending on the required statistics [25]. The absorbed doses are calculated from the energy-dependent fluence rate data and kerma factor data for each radiation dose component [30]. The same beam model can be used in both TPSs. BNCT_Rtpe and SERA use neutron and photon cross section data from the ENDF-IV/V/IV libraries that was pre-processed into 94 neutron energy groups: 22 thermal neutron groups (E<0.414 eV), 40 epithermal neutron groups (0.414 eV <E< 9.12 keV) and 32 fast neutron groups (9.12 keV <E< 16.9 MeV) [57]. The spatial doses, fluences and activation reaction rates are tallied into the 3D virtual subelement mesh that is composed of 30*30*30 cubic voxels (cube side 10 mm). In SERA, both the subelement number and the voxel size can be changed [57]. However, the use of smaller voxel sizes increases the computation time if the statistical uncertainty of the results is kept constant.

4.1 Beam model geometry

The neutron-photon beam model of the FiR(K63) beam for the BNCT_Rtpe/SERA was determined from the DORT beam model with the water phantom. The beam model of the 11-cm and the 14-cm beams were defined in a similar manner for the TPS. The beam model of the TPS is an averaged source plane over the airspace and was defined 5.0 cm inwards from the beam exit plane (Study IV). The beam description includes the neutron and photon spectra of the 47-neutron and 20-photon BUGLE-80 energy groups [41] and angular distributions of all 67 energy groups in 10 cosines of equal probability direction from 1 to 0 [30] (Figure 8). In addition to the spectral description, the TPS beam model includes a geometric description i.e. the disk-shape beam plane and the 5-cm-thick conical Li-polythene collimator. The collimator and the phantom were defined in the TPS with logical combinations of geometric primitives (cylinder, cone…) [30].

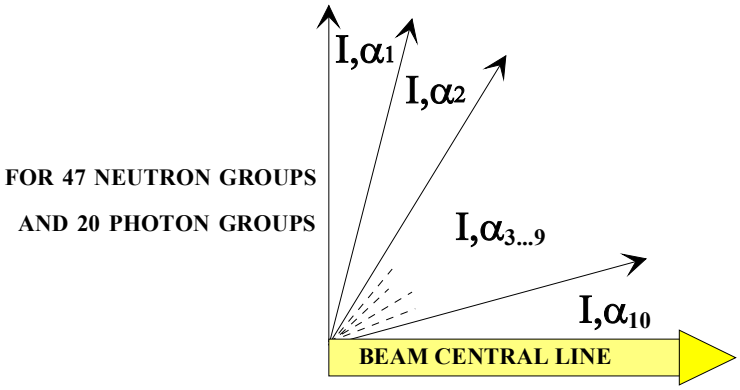

Figure 8. *Neutron-photon beam description in TPS. Ten angular directions of the equal probability current (I) are described at cosine cut-points (cosα) for 47 neutron and 20 photon energy groups.*

4.2 Verification in phantoms

The thermal neutron fluence has usually been determined with activation measurements, and gamma D_g and the fast neutron doses D_{fast_n} with pair ionisation chambers [18, 49, 52]. Kosunen *et al.* (Study III) ended up determining total neutron dose D_n instead of the fast neutron dose D_{fast_n} in a phantom. In BNCT treatment planning, the same weighting factor (also called RBE in literature) has been used world wide for nitrogen and fast neutron dose components D_N and D_{fast_n} [11, 24]. Therefore, these dose components have not required separate verification with measurements.

In BNCT_Rtpe and SERA, D_N and D_{fast_n} are printed out separately [57]. In addition, the neutron dose component known as the "other dose" can be printed in SERA. The "other dose" includes absorbed neutron doses from carbon and oxygen in tissue at the fast neutron energies [57]. The neutron dose from other minor isotopes (Na, P, S, Cl, K) in brain tissue [8] is negligible [58]; therefore, the total neutron dose in SERA is a sum of D_N, D_{fast_n} and the "other dose". The total gamma dose D_g in the BNCT_Rtpe and SERA programs consists of the hydrogen capture gamma dose $D_{g,H}$ and the beam gamma dose $D_{g,beam}$. In BNCT, the other (n,γ) reactions in tissue occur at such a low probability that they make no significant contribution to the gamma dose in tissue, and thus, are not included in D_g in the BNCT_Rtpe and SERA programs [59]. Difference of the cross sections used in these TPSs is that the photon cross section data has been switched from ENDF/B-IV (BNCT_Rtpe) to ENDF/B-VI (SERA). This change brought about 3-5% reduction in D_g in SERA as compared with in BNCT_Rtpe [60].

The initial SERA computations of the absorbed dose components in the water phantom showed that the amount of the thermal neutron-induced dose $D_N + D_{g,H}$ varied between 90% and 95% at depths of 0.5-10 cm of the water phantom in the 14-cm FiR(K63) beam. The rest of the absorbed total dose in the water phantom consists of $D_{g,beam}$., D_{fast_n} and "other dose", and their respective portions are 2-5%, 2-7% and <1% at depths of 0.5-10 cm. The doses reported here were computed for adult brain tissue as defined by ICRU 46 [8]. Since the thermal neutron-induced doses in the brain tissue substitute (TS) phantom predominate, it is important to validate the thermal neutron fluence distribution in a TS phantom. However, the total gamma and neutron doses D_n and D_g in a phantom also need to be validated to assure the non-thermal neutron fluence-induced dose distributions as well as the correctness of the dose computations in the TPS.

The FiR(K63) beam models and the computations of the BNCT_Rtpe were experimentally validated in the three homogeneous phantoms (Study IV). The diluted Au-Al activation foil measurements were completed with the diluted Mn-Al foils as described earlier (section 3.2). When either the diluted Au-Al or Mn-Al foil was excluded from the phantom model, the disruption to the activation reaction rate $r_{Au\text{-}197}$ or $r_{Mn\text{-}55}$ was computed in the DORT model to be negligible (0.2%). Thus, the modelling of the foils in a phantom geometry was demonstrated to be unnecessary. This was convenient because the foil size was very small (0.023 cm^3), and to get a good statistical result in a small volume would require a remarkably long computing time. In addition, only the fixed subelement mesh (1-cm^3 voxel) was available in the BNCT_Rtpe software, therefore, the result inside the small size foil would vanish in the averaged result of the relatively large unit voxel. The default 1-cm^3 voxel was used in both programs.

The Monte Carlo based treatment planning program SERA has an option to compute $r_{Au\text{-}197}$ and $r_{Mn\text{-}55}$. Therefore, the same beam normalisation method can be used as for the DORT computation. In BNCT_Rtpe, this option was specially tailored to our group (Study IV). The statistical analysis at the normalisation point at a depth of 2.0 cm in the PMMA phantom was computed in SERA for the activation reaction rates and the doses to estimate the need of histories to follow, since the program do not print the point statistical errors. This analysis was possible since the computation times with SERA were reasonable. The analysis showed (Figure 9) that at least 25 million histories were needed in a calculation to achieve a better than 0.5% statistical uncertainty for $r_{Au\text{-}197}$ and 5 million histories for $r_{Mn\text{-}55}$ at the thermal neutron maximum. However, 50 million histories were needed to have the same normalisation factor of 0.94 from both activation reactions. Lower number of histories, at least 5 million, were needed to obtain a 0.5% statistical uncertainty of the dose components, except for the fast neutron dose D_{fast_n}, which required four times as many histories to follow. This was due to D_{fast_n} being very low (3% of the total dose at a 2.0-cm depth). In SERA, 50 million histories were chosen to be followed in a simulation to compute the activation reaction rates and 20 million to compute the absorbed doses in a phantom. Since both results are computed in one computer run, 50 million histories were used for the phantom computations of the beam validation and normalisation, which takes 17 hours by the SUN Ultra 60 computer. However, for the optimisation of the field arrangement in the BNCT treatment planning, 0.5 million histories for a field have been found satisfactory, and the computation takes only 10 minutes of computer time. The final doses for the BNCT treatment plan are computed using 5 million histories per field in SERA.

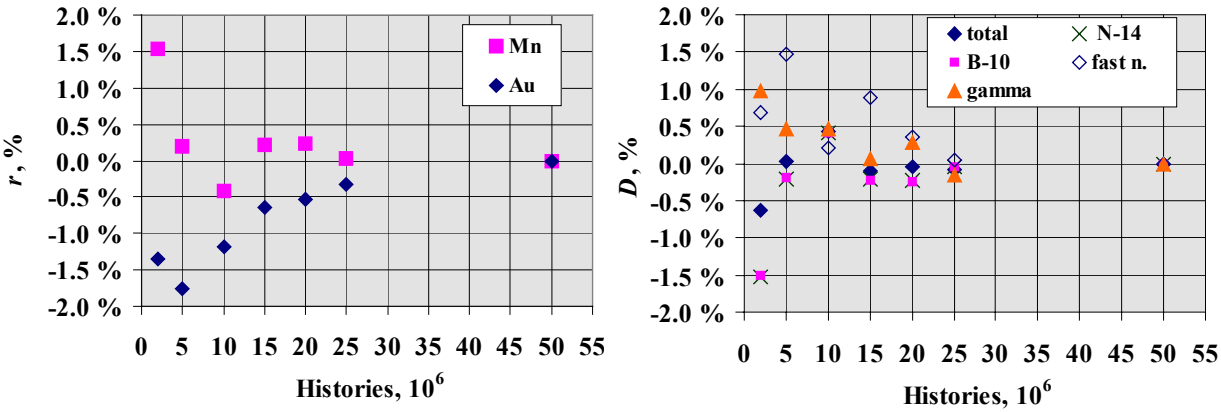

Figure 9. *Statistical analysis in SERA for the activation reaction rates r and the absorbed doses D at the thermal neutron maximum (depth 2.0 cm) in the PMMA phantom of the FiR 1 14-cm beam.*

The comparison of the calculated and the measured $r_{Au\text{-}197}$ and $r_{Mn\text{-}55}$ showed a good agreement in three cylindrical phantoms (Figure 10). Only at the beam entry point were the calculated $r_{Au\text{-}197}$ or $r_{Mn\text{-}55}$ 6-19% higher than the measured. This is due to 1-cm^3 (default value) subelement voxels being used and the interpolation in the air-phantom material interface being inaccurate (Study IV). The results of the comparison were similar for the 11-cm-diameter beam and for the BNCT_Rtpe computations. In the DORT calculation (Figure 7) where the foil-size tally voxel was modelled on the surface of the phantom, the calculated $r_{Au\text{-}197}$ or $r_{Mn\text{-}55}$ were 5% lower than the measured ones. The ascending C/E ratios as a function of depth observed in connection to the DORT calculations were not observed here. This can be explained by the thermal neutron cross sections being presented in 22 energy groups in SERA and BNCT_Rtpe compared with the two groups in DORT computations.

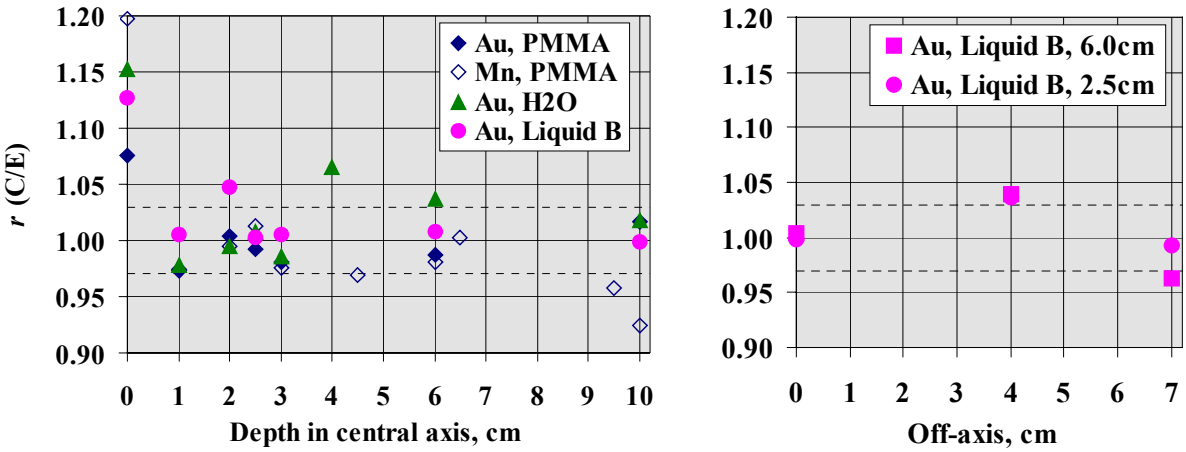

Figure 10. *Ratio of calculated (SERA) and experimental (C/E) $^{197}Au(n,\gamma)$ and $^{55}Mn(n,\gamma)$ activation reaction rates r in three cylindrical phantoms in the 14-cm beam. The dotted lines describe the measurement uncertainty 3% (1SD).*

The comparison of the calculated $r_{Au\text{-}197}$ and $r_{Mn\text{-}55}$ with the measured ones describes the quality of neutron spectra at the measurement location. When ratios of the calculated and the measured $r_{Au\text{-}197}$ and $r_{Mn\text{-}55}$ are the same for these two reactions, the neutron spectrum in the thermal neutron energy area can be assumed to be correct. Since the calculation and the measurement of $r_{Au\text{-}197}$ and $r_{Mn\text{-}55}$ are independent of each other, the comparison is reliable. Therefore, the first priority is to validate the thermal neutron spectrum with the ^{197}Au(n,γ) and the ^{55}Mn(n,γ) activation reaction rates. Moreover, it is convenient to print out the calculated and measured thermal neutron fluences and compare them, but one should note that a spatially calculated neutron spectrum in 47 energy groups was assumed to determine the measured thermal neutron fluence rate ϕ_{th}. The measured ϕ_{th} was determined by using $r_{Au\text{-}197}$ as described in section 3.2. Figure 11 compares the measured ϕ_{th} to the computed ones in the water phantom using the DORT model and the BNCT_Rtpe (rttMC) and SERA treatment planning programs. The calculated values were normalised to the Au-Al activation foil measurements at the reference monitor unit rate $\dot{MU}_{\mathrm{Re}f}$ in the PMMA phantom, at a depth of 2.0 cm, in each program separately. The calculations and the measurements were in a good agreement, except at the surface of the phantom using BNCT_Rtpe and SERA, where the computed fluence was overestimated by 39% and 36%, respectively.

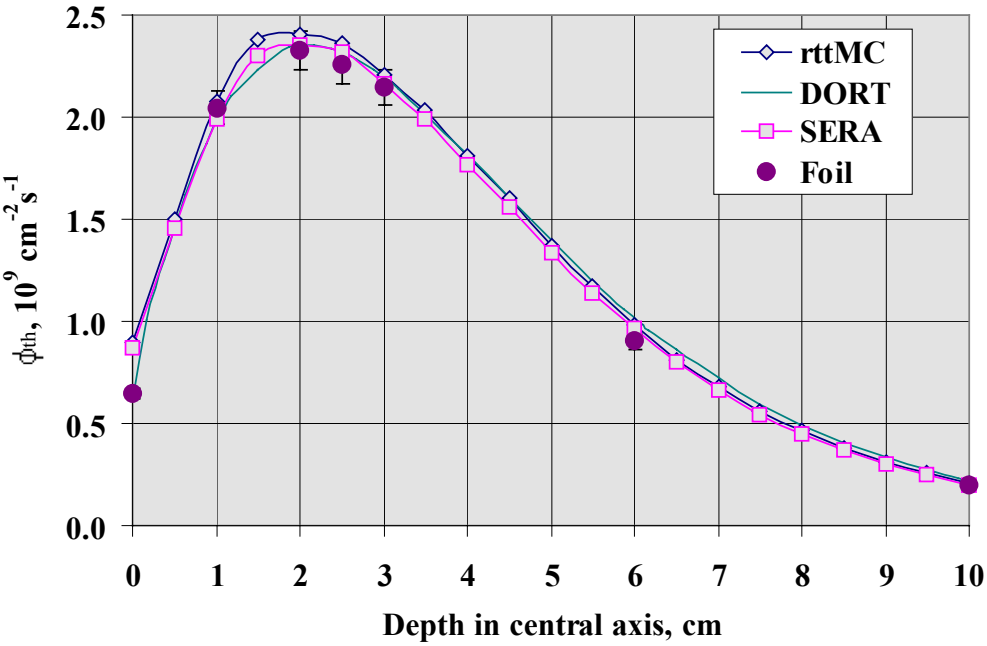

Figure 11. *Thermal neutron fluence rates (E<0.414 eV) ϕ_{th} in the central axis of the cylindrical water phantom in the 14-cm FiR(K63) beam. Error bars represent 4.0% uncertainty of measured values.*

The method to measure the total neutron dose D_n and the total gamma dose D_g in NCT was established in Study III. The calculated spatial neutron energy spectra in the phantoms were required to determine the measured D_n. The spatial neutron spectra were computed in the DORT model in BUGLE-80 energy groups. The IC measurements [44] were used to verify the computed D_n and D_g in the three homogeneous phantoms. Figure 12 compares the measured total neutron and total gamma dose rates with the computed ones using the DORT model and the BNCT_Rtpe (rttMC) and SERA. The calculated values were normalised to the activation measurements in each program separately as neutron fluences. The small difference in D_g in the TPSs was explained with the different version of the ENDF cross section library [60]. In addition to our group measurements, an excellent agreement of the computed (BNCT_Rtpe) and the measured boron dose D_B in the 11-cm FiR(K63) beam was demonstrated by the INEEL dosimetry group in their comparable measurements [17].

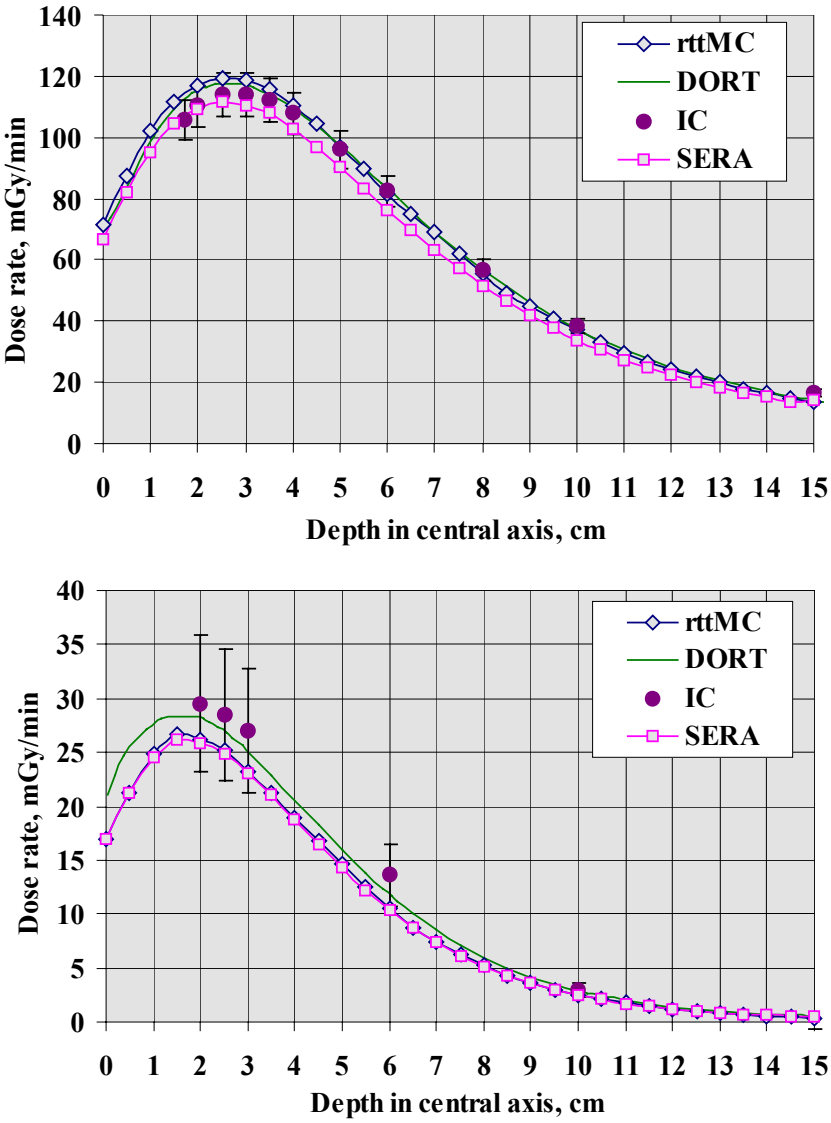

Figure 12. *Total gamma (above) and neutron (below) dose rates at the central axis in the cylindrical water phantom in the 14-cm FiR(K63) beam. Error bars represent 6.3% (gamma) and 21.5% (neutron) uncertainties of measured doses (Study III).*

4.3 Normalisation of beam model

Previously, at MITR-II [14] and at HFR [58], the TPS calculations in BNCT were normalised in approximately human head sized phantoms. The calibration phantom was a PMMA cube (size 15 cm) [58] or a water-filled, thin acrylic ellipsoid [14]. At HFR, the BNCT_Rtpe calculations were normalised to a 2-cm depth in the calibration phantom with a 2200 m/s (0.0253 eV) fluence rate [58] determined using the two-foil method (Au-Al (5 w-% Au) and Mn-Ni (88 w-% Mn)) [53, 58]. At MITR-II, where the NCTPLAN [14] was used as a TPS, all the dose components were calibrated separately based on the paired ionisation chamber measurements in the calibration phantom [14, 49]. Both facilities used a beam monitor system.

The beam models of the FiR 1 were normalised to a 2-cm depth, i.e. at the thermal neutron maximum in the PMMA phantom (diameter 20 cm, length 24 cm), by the ratio of the measured and the computed ^{197}Au(n,γ) activation reaction rates at the reference monitor unit

rate (Study IV). The PMMA phantom was chosen as a calibration tool as described in section 3.1.

The use of ^{197}Au(n,γ) activation reaction rate $r_{Au\text{-}197}$ for the normalisation of an epithermal neutron beam in a phantom were justified because the uncertainty of $r_{Au\text{-}197}$ is small (3% 1SD), and the computed and the measured activation reaction rates are independent of each other. The small size of foils (diameter 12 mm, thickness 0.2 mm) could be modelled as a phantom material because their effect on reaction rates were negligible (0.2%). This was very important for the Monte Carlo based treatment planning computations described in section 4.2.

The ^{55}Mn(n,γ) activation reaction rate $r_{Mn\text{-}55}$ would be the first choice to normalise the calculations since the energy response is mainly in the area of thermal neutrons (Figure 6), which induce most of the absorbed doses. However, the activation cross section data of the ^{197}Au(n,γ) from IRDF-90 [55] are better known with <1% uncertainty, whereas the uncertainty of the ^{55}Mn(n,γ) cross sections is < 4.5% at the energy area of interest.

The ^{197}Au(n,γ) and ^{55}Mn(n,γ) activation reaction rates $r_{Au\text{-}197}$ and $r_{Mn\text{-}55}$ were examined using different simulation programs and two cross section data of SERA. The two cross section data used in SERA were from the 640-group IRDF-90 library [55]. The only difference in these condensed 94-group cross sections for SERA was that a different weighting spectrum was used. The original data of SERA is called "SERA orig. c.s." and another cross section data is named "SERA VTT c.s.". The weighting spectrum for "SERA VTT c.s.", described in Study IV, is used in the computations in SERA and in BNCT_Rtpe at FiR 1. The calculated values were compared with the experimental ones in the central axis of the PMMA phantom (Figures 13 and 14). In addition to the previously presented computations, the reaction rates were computed using the MCNP program [29], which uses the continuous ENDF-VI cross section library. The SERA/BNCT_Rtpe neutron beam model was also used in MCNP. The calculated values were not normalised to compare only the computational effects between the programs.

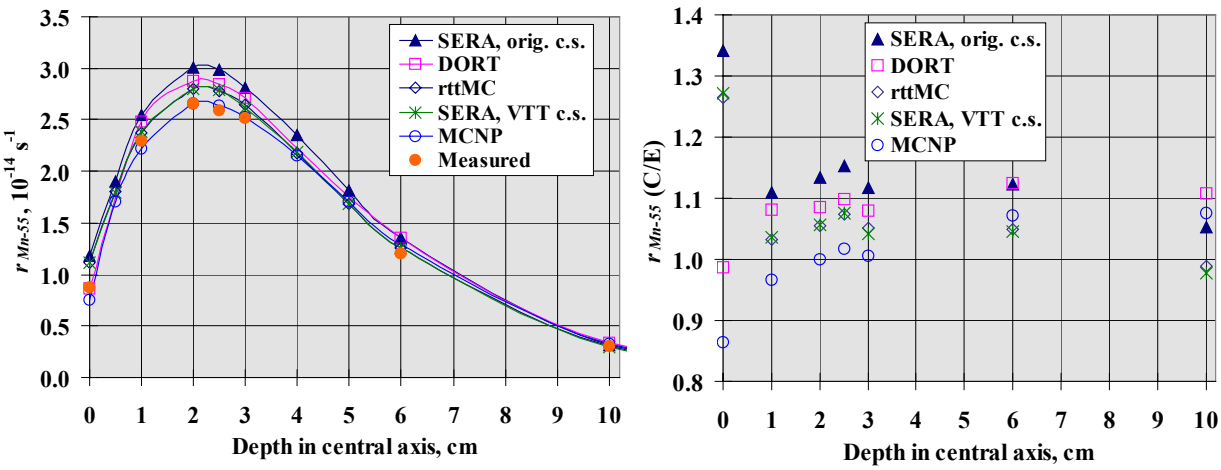

Figure 13. *Calculated and measured ^{55}Mn(n,γ) activation reaction rates $r_{Mn\text{-}55}$ in the cylindrical PMMA phantom in the 14-cm beam (left). Ratios of the calculated $r_{Mn\text{-}55}$ using different programs are compared with experimental values (C/E) (right).*

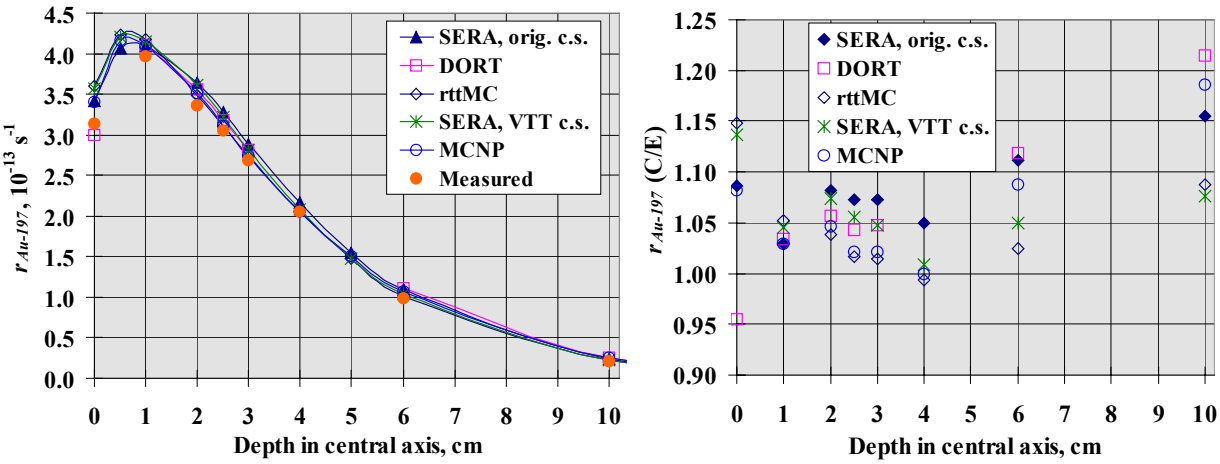

Figure 14. *Calculated and measured $^{197}Au(n,\gamma)$ activation reaction rates r_{Au-197} in the cylindrical PMMA phantom in the 14-cm beam (left). Ratios of the calculated r_{Au-197} using different programs are compared with experimental values (C/E) (right).*

r_{Mn-55} was more program- and cross section-dependent than r_{Au-197}. r_{Au-197} computed in SERA with the original cross sections was 13% higher than in MCNP and 7% higher than in another set of cross sections (SERA VTT c.s.) in SERA at a depth of 2.0 cm. The corresponding r_{Au-197} in SERA was 3% higher compared with MCNP, and the effect of the two cross section sets in SERA was only 1%.

This study proved that r_{Au-197} was less independent of the grouped cross section data and of the simulation programs than r_{Mn-55}. In addition, the uncertainty of the ^{197}Au(n,γ) cross sections (<1%) was lower than that of the ^{55}Mn(n,γ) reaction (<4.5%) in the IRDF-90 library [55]. As a consequence, r_{Au-197} is a preferable activation reaction for beam normalisation in the TPS. The normalisation factor of the FiR(K63) beam model in SERA was found to be the same, 0.94, with both activation reactions (Figure 9), which indicated that the neutron spectrum was correct at the normalisation depth of 2.0 cm. The normalisation of the beam model to the measured r_{Au-197} gives the link to the reference monitor unit rate $\dot{MU}_{Ref}$. All the irradiations that are provided according to the dose plan are given in monitor units at the FiR 1 facility.

5 TREATMENT PLANNING IN NCT

5.1 Principles

The purpose of the BNCT treatment plan is to achieve an optimised geometrical set-up of neutron fields relative to the patient and the monitor units connected to each field. The geometrical set-up consists of a selection of numbers, sizes, directions and weights of fields. The monitor units per field involve a planned radiation dose and a ^{10}B concentration in whole blood during the irradiation from one field. Optimisation of the treatment plan set-up in the Finnish clinical protocols is based on the following [13]: 1) a possible flat and high radiation dose distribution to PTV, 2) an avoidance of the radiation dose in the contralateral hemisphere and 3) maintaining doses under the pre-set dose maximum in the radiosensitive tissues of a patient.

A 3D geometrical model of a target is created to compute the radiation doses in the TPS [14, 30]. In the Finnish studies, the construction of the head model has been based on MR images (Studies VI, VII). The structures from the images are outlined based on either the non-uniform rational B-Spines (NURBS) technique (in BNCT_Rtpe) [30] or pixel-by-pixel uniform volume element (univel) reconstruction (in SERA) [61].

The weighted dose in PTV, tumour and normal brain of the patient's head is calculated from Equation 2. The prescribed weighted dose D_W is given to a patient in monitor units MU (Study VII)

$$MU = \frac{D_W}{\dot{D}^{calc}_{\mathrm{Re}f}} \dot{MU}_{\mathrm{Re}f}, \tag{3}$$

where $\dot{D}^{calc}_{\mathrm{Re}f}$ is the calculated dose rate at the reference monitor unit rate $\dot{MU}_{\mathrm{Re}f}$. MU is a reading of the ^{235}U fission chamber that measures epithermal and thermal neutrons in the beam collimator [56].

During irradiation Mn-Al foils are irradiated on a patient's head and TLD pellets on the head and body, and after that the detectors are analysed [62]. The ^{55}Mn(n,γ) reaction rates and the gamma doses of these *in vivo* measurements of the head are compared with the corresponding values in a treatment plan (Study VII). Suitable TLDs and analysing techniques were examined in Study V. The gamma dose was measured with MCP-7s TLDs, which have a low thermal neutron sensitivity. Based on the calculated neutron spectrum at the measurement location, the thermal neutron sensitivity of the MCP-7s detector is reduced (Studies V, VI).

5.2 Dog brain model

To improve patient safety and determine the radiobiological characteristics of the FiR(K63) beam, single-fraction dose-response studies were carried out on dog brains before clinical trials. The dose-planning procedure and the uncertainties of the dose plan were examined without the boron carrier (Study VI). BNCT_Rtpe was used for the dose planning. Irradiations were monitored with *in vivo* dosimeters, as recommended in BNCT of brain tumour patients.

According to the dosimetric study (Study VI), the estimated uncertainties (1 SD) of the calculated absorbed gamma, nitrogen and fast neutron doses were 9.6%, 5.8% and 36%, respectively, at the thermal neutron maximum in brain tissue. The uncertainty (1 SD) of the total absorbed dose from these dose components was 8.9%. The largest source of uncertainty for the dose components in tissue, based on the measurement uncertainties, was the beam model. The uncertainty of the gamma dose validated with IC measurements (Study III), in particular, had a great influence on the uncertainty of the computed total dose in brain tissue in NCT.

The examination, especially *in vivo* measurements and their comparison to calculations, brought out important information about the TPS for clinical trials. The measurement locations were in the beam entry on the top of the head, between the eyes and in the mouth at the border of the soft and hard palate and at the level of the oral cavity. At beam entry, the calculated thermal neutron fluences and the $^{55}Mn(n,\gamma)$ activation reaction rates were overestimated by 20% as in the phantom studies, which was due to the interpolating difficulties of the TPS in the air-tissue interface. Near the air cavities, between the eyes and in the mouth, the computations in the TPS were less accurate. The difference of the calculated neutron fluence and gamma dose to the measured ones was observed to vary 40-70%. The uncertainties (1 SD) of the calculation at the measurement point in the mouth were large (37-65%), which was principally caused the 10 mm uncertainty (1 SD) in a detector location. However, since the $^{55}Mn(n,\gamma)$ reaction rate mainly from the thermalised neutrons in the head agreed at the beam entry as in the phantom studies, the thermal neutron fluence (nitrogen dose) and the induced gamma dose most probably were within the above-mentioned uncertainties at the thermal neutron maximum. The dose in the thermal neutron maximum (1 cm^3), i.e. the peak dose, is usually used as a base to compute the given monitor units [11, 13].

The dosimetry chain of this examination was found to be sufficiently reliable to continue to clinical trials. The uncertainty of the calculated absorbed total dose without the uncertainty in the boron concentration at the thermal neutron maximum in brain tissue was below 10%. In addition, the delivered absorbed dose has metrologically traceable links to the international dosimetry standards [63]. In connection to the radiobiological characterisation of the beam, the dose planning of 20 cases, starting from the MR images to the given monitor units, provided an important foundation for the BNCT dose planning.

5.3 Glioblastoma patients

The first clinical BNCT protocol (P-01) for glioblastoma multiforme (GBM) brain tumour patients started at the FiR 1 facility in May 1999 [13], and the second protocol (P-03) for recurrent GBM patients in February 2001. The treatment planning in protocol P-01 was done with the BNCT_Rtpe program, and in protocol P-03 with the SERA program. Before starting to use SERA in protocol P-03, the TPS was verified and validated in the phantoms, and ten BNCT_Rtpe treatment plans of the protocol P-01 were recalculated with SERA [60].

For treatment planning, an individual approximate model of the irradiated target (head of GBM patient) is created based on transaxial MR images (Study VII). A minimum of three MRI-visible markers are taped on the skin surface for MR imaging, and the position of the markers in the MR images of the head model are used for patient positioning [26]. The computational head model consists of the skin, skull, brain, PTV and tumour region in protocol P-01. In addition to these structures, the air cavities were also outlined in protocol P-

03. Since the image data are inadequate to define the individual tissue compositions in BNCT, the compositions were defined after literature based on the ICRU 46 Report [8] (Study VII). At the HFR treatment planning of glioma patients in BNCT, the skull of the head was not modelled separately in the head model [64]. In the FiR(K63) beam, the lack of skull in the human head model increased the total weighted peak dose rate by 4-5%, and the peak was transferred by the thickness of skull towards the surface direction. For these reasons, the skull was required for inclusion in the head model in the BNCT treatment planning. The physical doses (i.e. fluence-to-kerma) are computed to the adult brain tissue defined by ICRU 46 (Study VII). In contrast with Study VII, the fluence-to-kerma conversions of the weighted dose components are calculated in the brain tissue using the brain tissue composition (equal amounts of white and grey matter) defined by Brooks *et al.* [65]. This tissue composition was used in the dose determination of the radiobiological studies when the weighting factors of 3.2 for fast neutron and nitrogen doses and of 1.0 for the gamma dose were determined in the BMRR beam [24] and was applied with the factors in our BNCT dose computations.

The uncertainty of the absorbed peak dose of the brain cancer patient in BNCT in the FiR(K63) beam can be estimated approximately from the dose uncertainties based on the dog head model in NCT (Study VI). The chains of the dog brain NCT and the human brain cancer patient in BNCT starting from the MR images of the dose plan to the irradiation set-up are analogous. Their major processional difference is the use of the boron carrier in BNCT and its absence in NCT. In BNCT, so far the boron concentration in tissue is estimated to be homogeneous in the TPS. The defined ^{10}B concentration in tissue is based on the tissue-to-whole-blood ratio of the ^{10}B concentration that is estimated from the biological models [24]. The uncertainty of the boron dose is estimated to be equal to the uncertainty of the computed nitrogen dose of 6% (1SD), since both doses are directly proportional to the thermal neutron fluence. The uncertainty of the boron dose D_B does not include the uncertainty of the boron concentration in tissue, which is part of future BNCT research world wide. The uncertainty of the computed gamma dose D_g was estimated to be 10% (1SD), and the uncertainty of the computed fast neutron dose D_{fast_n} 36% (1SD) at the thermal neutron maximum in brain tissue (Study VI). In one hour irradiation, the typical absorbed dose components at the thermal neutron maximum in normal brain tissue are 5.3 Gy, 5.0 Gy, 0.9 Gy and 0.2 Gy for D_B, D_g, D_N and D_{fast_n}, respectively, at a 12 ppm ^{10}B concentration blood level in a patient (Study VII). From the dose contributions and dose uncertainties, the uncertainty of the computed absorbed total dose can be estimated to be 8% (1SD) without uncertainty in boron concentration at the thermal neutron maximum in the brain tissue of a patient in the FiR(K63) beam. Recently, Kortesniemi [40] estimated in his Ph.D. thesis a 30% (1 SD) uncertainty in boron concentration in normal tissue. When taking this boron concentration uncertainty into account, the uncertainty of the computed absorbed total dose is 20% (1 SD) in the normal brain.

During the irradiation of each field Mn-Al foils are irradiated on a patient's head and TLD pellets (MCP-7s) on the head and body, and after treatment the detectors are analysed [62]. The ^{55}Mn(n,γ) reaction rates and the gamma doses of these *in vivo* measurements of the head are compared with the corresponding values in a treatment plan. The value of *in vivo* dosimetry in BNCT is to verify the computed doses. The *in vivo* measurements in the first protocol (P-01) led to the observation that when including the air cavities in the head model the calculated neutron dose distribution in the frontal part of the head was markedly enhanced in the posterior–anterior field (Table 5). However, the more precise head model had no influence on absorbed dose components at the thermal neutron maximum; nor did it have a

strong effect on gamma doses (Table 6). Based on these *in vivo* measurements, the air cavities of the head should be included in the anatomic model of the patient head in BNCT.

Table 5. *Comparison of measured $^{55}Mn(n,\gamma)$ reaction rates $r_{Mn\text{-}55}$ with calculated values (C/E) in two head models of the same patient with and without inclusion of air cavities in the model.*

Location	Measured $r_{Mn\text{-}55}$, 1/s	C/E, no air cavities	C/E, air cavities
Beam entry point	6.44E-15	1.24	1.17
Beam side ear canal	1.05E-15	0.69	0.81
Between eyes TAT	4.38E-17	0.20	0.51

Table 6. *Comparison of measured gamma doses D_g with calculated values (C/E) in two head models of the same patient with and without inclusion of air cavities in the model.*

Location	Measured D_g, mGy	C/E, no air cavities	C/E, air cavities
Beam opposite TAT	200	0.86	0.93
Beam side ear canal	260	1.04	1.00
Between eyes TAT	100	0.93	0.94

6 DISCUSSION

The 2D cylinder symmetrical horizontal DORT model of the FiR 1 beam was observed to be an effective and reliable tool for examining the effects of different geometrical structures (moderator, collimator, shielding) on neutron and photon spectra. The full neutron and photon spectra in the 47-neutron and 20-photon BUGLE-80 energy groups were achieved in the whole moderator-collimator part of the model in 60 minutes with a 0.01% flux convergence criterion in each energy group (SUN Ultra 60 computer). The changes in the beam geometry were verified primarily with activation measurements, and the corresponding changes in the DORT model were found to be reliably computed. The previously detected [32, 33, 46] 30-50% fast neutron underestimation in the aluminium-oxygen moderated epithermal neutron beam model was not observed in the aluminium-fluorine moderated beam model. Therefore, no spectral correction to the FiR(K63) beam model was required. The detailed 2D model of the reactor core, where a similar type of fuel elements was divided into the separate zones and the graphite reflector density was decreased due to air-filled structures in the beam direction, appeared to provide a more accurate model.

The Code of Practice for NCT dosimetry is currently under construction [35]. A method to determine the beam model for the treatment planning of brain cancer patients in NCT was developed for the FiR(K63) epithermal neutron beam. Suitable brain tissue substitute phantom materials are required to validate the thermal neutron fluence Φ_{th}, to which the boron D_B and nitrogen doses D_N are directly proportional, and the total neutron D_n and total gamma dose D_g distributions in a situation similar to patient radiation therapy. The parallel verification of the computed distributions of the dose components in the slightly different brain tissue substitute phantoms confirmed that the continuous neutron-photon spectra of the beam were correctly modelled. In the collimated FiR(K63) beam, PMMA was found to simulate Φ_{th} in the brain tissue 3 percentage units closer than water, which was opposite to the situation in the uncollimated epithermal neutron beam (Study II). Water simulates D_g in the brain tissue approximately 10 percentage units closer than PMMA in the uncollimated and the collimated epithermal neutron beams. PMMA is more suitable for the beam model normalisation to the activation measurements than water because of its superior ability to simulate Φ_{th} in the brain tissue. PMMA is also more practical than water in the measurements because the detector place can be defined more accurately in solid material than in liquid, and detector-supporting materials, which may disturb the neutron spectrum, are not needed. In the accelerator-based epithermal neutron beam, A-150 plastic was computed to simulate D_g in the brain tissue 9 percentage units closer than PMMA [66]. At the thermal neutron maximum, i.e. the beam normalisation point, A-150 and PMMA simulated Φ_{th} in the brain tissue equally, therefore, both are suitable for beam normalisation.

Activation measurements are the primary measurement technique in NCT since the uncertainty of $r_{Au\text{-}197}$ and $r_{Mn\text{-}55}$ is only 3% (1SD), which is considerably lower than uncertainties in ionisation chamber measurements (6.3% (1SD) for D_g and 21.5% (1SD) for D_n, Study III). The use of activation measurements in the experimental validation of the computations was relevant since the calculated thermal neutron-induced doses in the FiR(K63) beam were 90-95% of the total dose, from 0.5-cm to 10-cm depth, in a water phantom. The parallel use of the ^{197}Au(n,γ) and ^{55}Mn(n,γ) reactions in the validation of the computations in a phantom gave more reliability to computed neutron spectra. The measured and computed activation reaction rates are independent of each other, especially when diluted foils are used. The very diluted foils are practical to use since their disruption to $r_{Au\text{-}197}$ and

$r_{Mn\text{-}55}$ was negligible (0.2%) due to exceptionally low self-shielding. Therefore, the effect of the foils in dose calculations was insignificant and was not taken into account. This was especially important in the validation and normalisation of the beam model and the dose computations in the phantoms.

The ^{197}Au(n,γ) activation reaction rate $r_{Au\text{-}197}$ is recommended to normalise the beam model in a phantom, especially if the epithermal neutron beam has a low fast neutron and beam gamma contamination. Even thought the ^{55}Mn(n,γ) reaction produces a greater response (97%) in the thermal neutrons than the ^{197}Au(n,γ) reaction (58%) at the thermal neutron maximum in a PMMA phantom in the FiR(K63) beam, it is less suitable than the latter for normalisation. The computed $r_{Au\text{-}197}$ was less independent of the energy structure of the activation cross sections in the TPS than $r_{Mn\text{-}55}$. Furthermore, the uncertainties of ^{197}Au(n,γ) activation cross sections (< 1%) are lower than the uncertainties of ^{55}Mn(n,γ) activation cross sections (<4.5%) [55]. However, if the beam model is correct, the same normalisation factor is achieved with both activation reactions and no dose component related normalisation coefficients are needed. Although the neutron spectrum is correctly modelled and normalised, the beam gamma component might need a separate modification in the model. The future plan is to verify the beam model gamma spectrum.

The dose computations in the TPS were quite reliable in the homogeneous tissue but have shortages in the heterogeneous areas near air cavities and in other air-tissue interfaces, where the point doses are quite uncertain (Study VI). The soft tissues, skull and air cavities need to be outlined separately to get an accurate 3D head model for treatment planning. Enhanced reliability in the dose computations can be achieved if the continuous cross section data and variable sizes of tally voxels are included in TPS. This would particularly reduce the uncertainty of the calculated doses/activation reaction rates on the skin and near the air cavities. As a consequence, the validation of the computed doses in a head model with *in vivo* measurements becomes even more reasonable.

The main uncertainty of the calculated dose in NCT arises from uncertainties in measurements used to configure the beam model in a phantom. Therefore, the uncertainty of the computed doses can be reduced by developing the measurement technique of gamma and fast neutron doses in a phantom. The uncertainty of the computed BNCT total dose in the head model was estimated to be 8% at the dose maximum in brain tissue, assuming no error in boron concentration. This estimation is based on our study of the dog brain model (Study VI). The different computed dose components have their own (1SD) uncertainties; the fast neutron dose has the highest uncertainty of 36%, the gamma dose 10% and the nitrogen (boron) dose 6%. The uncertainty of the boron dose does not include the uncertainty of the boron distribution in tissue. Determination of boron distribution is a major part of future BNCT research world-wide.

The epithermal neutron beam model for TPS was validated for the brain tumour radiation therapy. Future NCT radiotherapy trials might extend to tumours other than those of the brain. When extracranial targets are treated with BNCT, the beam model in the TPS will need to be validated in a large-sized phantom. In this situation, the calculated dose distribution in the anatomic model should also be verified with *in vivo* dosimetry to give more reliabilily to the dose plan.

7 SUMMARY AND CONCLUSION

The beam model of the epithermal neutron beam is needed for computational dosimetry and treatment planning since all beams in NCT are individual. The model is validated experimentally in a situation similar to patient treatment. The thermal neutron fluence is most important to validate in a phantom since it induces the major portion of the absorbed doses in tissue. This is emphasised in the validation of the high-quality epithermal neutron beam, which has very low photon and fast neutron contamination in the beam, similar to the FiR(K63) beam. However, the total gamma and the total neutron doses in a tissue substitute phantom should be validated to ensure the reliability of the beam gamma-induced dose and the fast neutron dose in tissue and the dose computations of the TPS.

Study I describes the cylindrical horizontal DORT model of the FiR 1 epithermal neutron beam and the experimental validation of the calculated free beam neutron spectrum. The free beam model agreed well with the measurements in three neutron energy groups and fairly well with those 47 neutron energy groups. According to these measurements, the actual thermal neutron fluence was somewhat higher than the calculated fluence. However, upon more detailed analysis of the measurements, the experimental thermal neutron fluence approached the calculated values. The beam model was sufficiently accurate to be used in TPS.

Study II computationally examined suitable phantom materials for the NCT dosimetry. Two brain tissue equivalent liquids were designed from chemical compounds in addition to the simple materials (PMMA and water). Of the simple materials, water simulated the thermal neutron fluence and the gamma and fast neutron doses in the brain tissue better than PMMA in the uncollimated epithermal neutron beam.

The later computations in the collimated epithermal neutron beam FiR(63) showed that PMMA simulates the thermal neutrons in the brain tissue slightly better than water at the thermal neutron maximum. Because of this and the practicality of solid material in activation measurements, PMMA is the recommended material in epithermal neutron beam normalisation. However, water is superior to PMMA for simulating the absorbed gamma dose in brain tissue, therefore, the computed gamma dose is recommended for verification in a water phantom.

The pair ionisation chamber measurement method was developed to determine the total absorbed gamma dose and the neutron doses in a phantom for the NCT dosimetry in **Study III**. The measured and computed gamma and neutron doses agreed within the measurement uncertainties. The study gave more reliability to the calculated beam gamma and fast neutron dose distributions in a phantom. The overall uncertainties of the IC measurement technique in NCT dosimetry render it unsatisfactory as a primary measure of gamma and neutron doses in a phantom. In the high-quality epithermal neutron beam, the amount of absorbed gamma depth dose is 80-95% (0-10 cm) of the total dose, thus the 6.3% (1SD) measurement uncertainty in the gamma dose increases the uncertainty of the computed total dose in NCT most.

In **Study IV** the FiR(K63) beam model was defined for the treatment planning system. The beam model was defined from the DORT model of the FiR(K63) beam for each beam size separately. Each size was separately normalised at the thermal neutron maximum in the PMMA phantom with Au activation foil measurement. The $^{197}Au(n,\gamma)$ activation reaction was

observed to be less uncertain for the epithermal neutron beam normalisation than the $^{55}Mn(n,\gamma)$ reaction. The $^{197}Au(n,\gamma)$ reaction was found to be less independent of the energy grouping of the cross section data than the $^{55}Mn(n,\gamma)$ reaction in the TPS. The presently used TPS has drawbacks in the computation of surface dose, which is overestimated by approximately 10-20%.

Suitable TLDs and their thermal neutron reduction method were studied in **Study V**. The MCP-7s detector was observed to be suitable for measurements of the absorbed gamma dose in NCT. However, the method requires accurate data on the calculated neutron spectrum for the thermal neutron reduction at the measurement location. The significance of the MCP-7s detector in NCT is that it can be used in *in vivo* measurements to verify gamma doses of the computational model, especially because their small size and wirelessness.

The dose planning procedure and the uncertainties of the epithermal neutron-induced computed doses were examined in **Study VI**. The uncertainty of the computed total NCT doses was 9% at the thermal neutron maximum in the dog head model. During irradiation the calculated neutron fluences and the absorbed gamma doses were verified on the skin and in the mouth with *in vivo* measurements using Mn-Al activation foils and MCP-7s TLDs, respectively. The examination showed that in the homogeneous area on the top of the head the calculated doses had an equal overestimation than in a phantom, which predicts that the calculated dose accuracies were within the measurement uncertainties. However, the accuracy of the calculated point dose at air-tissue surfaces and near air cavities was insufficient.

Study VII described the chain of BNCT treatment planning for brain tumour patients from the dosimetric point of view. According to a sample BNCT dose plan, the weighted boron dose is approximately 90% of the total weighted dose for a tumour and 45% for a normal brain at the dose maximum. Therefore, experimental validation of the thermal neutron fluence that is directly proportional to the boron dose is essential in a phantom and in tissue with *in vivo* measurements to assure reliability of doses in BNCT.

ACKNOWLEDGEMENTS

The investigations presented in this thesis were carried out at the Finnish Research Reactor (FiR 1), Espoo. I wish to thank VTT Processes, NC-Treatment Ltd. and the Department of Physical Sciences, University of Helsinki, particularly Professor Juhani Keinonen, Head of the Department of Physical Sciences, for resources placed at my disposal.

I am deeply indebted to my supervisors, Docent Sauli Savolainen, Ph.D., and Iiro Auterinen, M.Sc.Tech., for guidance and support during the preparation of this thesis. Sauli taught me to focus on the essentials, and Iiro showed me the importance of thoroughness in research and deserves special thanks for believing in me when I lacked confidence in myself.

I warmly thank Professor David Nigg, Ph.D., who invited me to the Idaho National Engineering and Environmental Laboratory, USA, for guidance in reactor modelling and dose planning, and for valuable professional advice over the years. I also thank the late Floyd Wheeler, M.Sc., who taught me numerous things associated with the BNCT treatment planning system, and Charles Wemple, Ph.D., who advised me in questions dealing with SERA and MCNP. I am also grateful to Associate Professor Jacek Capala, Ph.D., who introduced me to the world of clinical BNCT treatment planning at the Brookhaven Medical Research Reactor, USA.

I am greatly indebted to Docent Mikko Tenhunen, Ph.D., and Docent Simo Hyödynmaa, Ph.D., for their professional reviews of the manuscript and constructive comments that have markedly improved this thesis.

I warmly acknowledge all the co-authors of the adjoining publications, especially Tom Serén, Lic.Tech., Jyrki Vähätalo, Lic.Phil., Carita Aschan, Ph.D., Mika Kortesniemi, Ph.D., and Antti Kosunen, Ph.D. In addition, the Finnish BNCT research group and the FiR 1 reactor staff are thanked for excellent assistance and support and for creating a nice atmosphere and inspiring coffee brakes. Particularly, I want to express my deep gratitude to Judit Benczik, Ph.D., Docent Markus Färkkilä, M.D., Ph.D., Professor Emeritus Pekka Hiismäki, D.Tech., Professor Heikki Joensuu, M.D., Ph.D., Karoliina Kaita, M.Sc.Tech., Merja Kallio, M.D., Ph.D., Leena Kankaanranta, M.D., Johanna Karila, M.Sc., Hanna Koivunoro, M.Sc., Petri Kotiluoto, M.Sc., Martti Kulvik, M.D., Juha Lampinen, Ph.D., Pertti Niskala, Docent Seppo Pakkala, M.D., Ph.D., Jussi Perkiö, M.Sc., Johanna Saarinen, M.Sc., Eero Salli, D.Sc.(Tech.), Seppo Salmenhaara, M.Sc.Tech., Petteri Välimäki, M.Sc., and Hanna Ylä-Mella, M.Sc. I am also grateful to my fellow workers at VTT Processes and in the HUS Department of Oncology. My sincere thanks to Carol Ann Pelli, Hon.B.Sc., for editing the language of the summary.

Finally, a warm thank-you to my friends and relatives, who took great care to ensure that my life outside of working hours was wonderful.

The financial support of the Academy of Finland, the State Subsidy for University Hospitals, University of Helsinki, NC-Treatment Ltd., the EC (A code of practice for dosimetry of Boron Neutron Capture Therapy (BNCT) in Europe, Contract No. SMT4-CT98-2145) and Tekes, the National Technology Agency of Finland, are gratefully acknowledged.

November 2002 Tiina Seppälä

REFERENCES

1. Perez, C.A. and Brady, L.W. Principles and practice of radiation oncology. 3rd ed. Philadelphia: Lippincott-Raven Publishers (1998).
2. Fowler, J.F. Nuclear particles in cancer treatment. Medical Physics Handbooks 8. Bristol: Adam Hilger Ltd (1981).
3. Hall, E.J. Radiobiology for the Radiologist. Philadelphia: J.B. Lippincott Company (1994).
4. Slatkin, D.N. A history of boron neutron capture therapy of brain tumours. Postulation of a brain radiation dose tolerance limit. Brain 114, 1609-29 (1991).
5. Attix, F.H. Introduction to radiological physics and radiation dosimetry. New York: John Wiley & Sons (1986).
6. Bewley, D.K. The physics and radiobiology of fast neutron beams. Medical Science Series. Bristol: Adam Hilger (1989).
7. Verbakel, W.F. and Stecher-Rasmussen, F. Determination of the γ-ray component of a neutron beam for medical irradiation application at the HFR in Petten. Nucl. Instr. Meth. Phys. Res. A 451, 676-84 (2000).
8. ICRU 46, Photon, Electron, Proton and Neutron Interaction Data for Body Tissues. International Commission on Radiation Units and Measurements. Bethesda, Maryland (1992).
9. ICRU 63, Nuclear Data for Neutron and Proton Radiotherapy and for Radiation Protection. International Commission on Radiation Units and Measurements. Bethesda, Maryland (2000).
10. Locher, G.L. Biological effects and therapeutic possibilities of neutrons. Am. J. Roentgenol. 36, 1-13 (1936).
11. Chadha, M., Capala, J., Coderre, J.A., Elowitz, E.H., Iwai, J., Joel, D.D., Liu, H.B., Wielopolski, L. and Chanana, A.D. Boron neutron-capture therapy (BNCT) for glioblastoma multiforme (GBM) using the epithermal neutron beam at the Brookhaven National Laboratory. Int. J. Radiat. Oncol. Biol. Phys. 40, 829-34 (1998).
12. Sauerwein, W. and Zurlo, A. The EORTC Boron Neutron Capture Therapy (BNCT) Group: achievements and future projects. Eur. J. Cancer. 38 Suppl. 4, 31-4 (2002).
13. Kankaanranta, L., Seppälä, T., Kallio, M., Karila, J., Aschan, C., Serén, T., Kortesniemi, M., Kotiluoto, P., Järviluoma, E., Kulvik, M., Laakso, J., Brander, A., Jääskeläinen, J., Vähätalo, J., Auterinen, I., Savolainen, S., Färkkilä, M. and Joensuu, H. First clinical results on the Finnish study on BPA-mediated BNCT in glioblastoma. In: Program and abstracts of 9th International Symposium on Neutron Capture Therapy for Cancer, October 2-6, 2000, pp. 31-2. ISNCT: Osaka (2000).
14. Zamenhof, R., Redmond II, E., Solares, G., Katz, D., Riley, K., Kiger, S. and Harling, O. Monte Carlo-based treatment planning for boron neutron capture therapy using custom designed models automatically generated from CT data. Int. J. Radiat. Oncol. Biol. Phys. 35, 383-97 (1996).
15. Moss, R.L., Aizawa, O., Beynon, D., Brugger, R., Constantine, G., Harling, O., Liu, H.B. and Watkins, P. The requirements and development of neutron beams for neutron capture therapy of brain cancer. J. Neurooncol. 33, 27-40 (1997).
16. Joel, D.D., Chadha, M., Chanana, A.D., Coderre, J.A., Elowitz, E.H., Gebbers, J-O. Liu, H.B., Micca, P.L., Nawrocky, M.M., Shady, M. and Slatkin, D.N.Uptake of BPA into glioblastoma multiforme correlates with tumor cellulary. In: Advances in Neutron Capture Therapy, Vol. 2, Larsson, B., Crawford, J. and Weinreich, R. (eds.), pp. 225-8, Elsevier Science B.V.: Amsterdam (1997).

17. Nigg, D.W., Harker, Y.D., Hartwell, J.K., Wemple, C.A., Serén, T., I., A., Kotiluoto, P., Hiismäki, P., Seppälä, T., Kortesniemi, M., Savolainen, S. and Risler, R., Collaborative neutronic performance characterization of the FiR 1 clinical epithermal-neutron beam facility for BNCT. In: INEEL BNCT Research Program Annual Report 1998, INEEL-EXT-99-00293, Venhuizen, J.R. (ed.), pp. 13-38, INEL/Lockheed Martin Idaho Technologies Company: Idaho (1999).
18. Raaijmakers, C.P., Konijnenberg, M.W. and Mijnheer, B.J. Clinical dosimetry of an epithermal neutron beam for neutron capture therapy: dose distributions under reference conditions. Int. J. Radiat. Oncol. Biol. Phys. 37, 941-51 (1997).
19. Yanch, J.C., Zhou, X.L., Shefer, R.E. and Klinkowstein, R.E. Accelerator-based epithermal neutron beam design for neutron capture therapy. Med. Phys. 19, 709-21 (1992).
20. Bleuel, D.L., Donahue, R.J., Ludewigt, B.A. and Vujic, J. Designing accelerator-based epithermal neutron beams for boron neutron capture therapy. Med. Phys. 25, 1725-34 (1998).
21. Green, S. Developments in accelerator based Boron Neutron Capture Therapy. Radiat. Phys. Chem. 51, 561-9 (1998).
22. ICRU 50, Prescribing, recording and reporting photon beam therapy. International Commission on Radiation Units and Measurements: Bethesda, Maryland (1993).
23. ICRU 42, Use of Computers in External Beam Radiotherapy procedures with High-Energy Photons and Electrons. International Commission on Radiation Units and Measurements: Bethesda, Maryland (1987).
24. Coderre, J.A. and Morris, G.M. Review: The radiation biology of boron neutron capture therapy. Radiat. Res. 151, 1-18 (1999).
25. Nigg, D.W., Wemple, C.A., Wessol, D.E., Wheeler, F.J., Albright, C., Cohen, M., Frandsen, M., Harkin, G. and Rossmeier, M. SERA - an advanced tratment planning system for Neutron Therapy and BNCT. Trans. Am. Nucl. Soc. 80, 66-8 (1999).
26. Seppälä, T., Kortesniemi, M., Kankaanranta, L., Perkiö, J., Auterinen, I. and Savolainen, S. Aspects of Dose Planning and Patient Positioning for BNC-Treatment at FiR 1. Med. Biol. Eng. Comp. 37, 402-3 (1999).
27. Auterinen, I., Hiismäki, P., Kotiluoto, P., Rosenberg, R.J., Salmenhaara, S., Seppälä, T., Serén, T., Tanner, V., Aschan, C., Kortesniemi, M., Kosunen, A., Lampinen, J., Savolainen, S., Toivonen, M. and Välimäki, P. Metamorphosis of a 35 year-old Triga reactor into a modern BNCT facility. In: Frontiers in Neutron Capture Therapy, Vol. 1, Hawthorne, M.F., Shelly, K. and Wiersema, R.J. (eds.), pp. 267-75, Kluwer Academic/Plenum Publishing Corporation: New York (2001).
28. Nigg, D.W., Randolph, P.D. and Wheeler, F.J. Demonstration of three-dimensional deterministic radiation transport theory dose distribution analysis for boron neutron capture therapy. Med. Phys. 18, 43-53 (1991).
29. Briesmeister, J.F. (ed.), MCNP - A general Monte Carlo N-particle transport code. Los Alamos National Laboratory Report LA-1225-M (1997).
30. Nigg, D.W. Methods for radiation dose distribution analysis and treatment planning in boron neutron capture therapy. Int. J. Radiat. Oncol. Biol. Phys. 28, 1121-34 (1994).
31. Auterinen, I. and Hiismäki, P. Epithermal BNCT neutron beam design for a Triga II reactor. In: The 5th International Symposium on Neutron Capture Therapy, Soloway, H., Barth, R.F. (eds.), pp. 81-4, Plenum Press: New York (1993).
32. Klee, K.A., Nigg, D.W. Wheeler, F.J., Karam, R.A. Conceptual Desing for an Advanced Epithermal-Neutron Beam for Boron Neutron Capture Therapy at Georgia

Institute of Technology Research Reactor. In: Proceedings of the 1994 Topical Meeting on Advances in Reactor Physics, Vol. 3, American Nuclear Society (1994).
33. Wheeler, F.J., Parsons, D.K., Rushton, B.L. and Nigg, D.W. Epithermal neutron beam design for neutron capture therapy at the Power Burst Facility and the Brookhaven Medical Research Reactor. Nucl. Tech. 92, 106-17 (1990).
34. Serén, T., Kortesniemi, M., Aschan, C., Seppälä, T., Lampinen, J., Auterinen, I. and Savolainen, S. A Tale of Two Beams - Comparison of the Radiation Fields at the BMRR and FiR 1 Epithermal BNCT Facilities. Med. Biol. Eng. Comp. 396-7 (1999).
35. Stecher-Rasmussen, F., Auterinen, I., Beddoe, A., Goncalves, I., Järvinen, H., Kosunen, A., Larsson, B., Marek, M., Mijnheer, B., Raaijmarkers, C.P.J., Savolainen, S., Voorbraak, W.P., Watkins, P. and Zsolnay, E. A code of practice for the dosimetry of BNCT in Europe. In: Advances in Neutron Capture Therapy, Vol. 1, Larsson, B., Crawford, J. and Weinreich, R. (eds.) pp. 237-40, Elsevier Science B.V.: Amsterdam (1997).
36. Rhoades, W.A. and Childs, R.L. The DORT Two-Dimensional Discrete Ordinates Transport Code. Nucl. Sci. Eng. 99, 88-9 (1988).
37. Aschan, C. Applicability of thermoluminescent dosimeters in x-ray organ dose determination and in the dosimetry of systemic and boron neutron capture radiotherapy. Ph.D. Thesis, Helsinki University, HU-P-D77 (1999).
38. Kosunen, A. Metrology and quality of radiation therapy dosimetry of electron, photon and epithermal neutron beams. Ph.D. Thesis, STUK - A164 (1999).
39. Benczik, J. Relative biological effectiveness of reactor produced epithermal neutrons for the canine brain. Ph.D. Thesis, Helsinki University (2000).
40. Kortesniemi, M. Solutions for clinical implementation of boron neutron capture therapy in Finland. Ph.D. Thesis, Helsinki University, HU-P-D95 (2002).
41. Roussin, R.W. BUGLE-80, Coupled 47-Neutron, 20-Gamma Ray, P_3, Cross Section Library for LWR Shielding Calculations. Radiation Shielding Information Center, Oak Ridge National Laboratory: Oak Ridge (1980).
42. Kaita, K., Serén, T. and Auterinen, I. First characterisation of the Finnish epithermal neutron beam using activation detectors. In: Advances in Neutron Capture Therapy, Vol. 1, Larsson, B., Crawford, J. and Weinreich, R. (eds.) pp. 353-6, Elsevier Science B.V.: Amsterdam (1997).
43. Nigg, D.W., Harker, Y.D., Hartwell, J.K., Wemple, C.A., Seppälä, T., Serén, T. and Auterinen, I. Collaborative spectral characterization of the Finnish epithermal-neutron beam facility for BNCT. In: INEEL BNCT Research Program Annual Report 1996, INEL/EXT-97-00319, Venhuizen, J.R. (ed.), pp. 15-32, INEL/Lockheed Martin Idaho Technologies Company: Idaho, (1997).
44. Kortesniemi, M., Kosunen, A., Aschan, C., Serén, T., Kotiluoto, P., Toivonen, M., Välimäki, P., Seppälä, T., Auterinen, I. and Savolainen, S. Measurements of phantom dose distribution at the Finnish BNCT facility. In: Frontiers in Neutron Capture Therapy, Vol. 1, Hawthorne, M.F., Shelly, K. and Wiersema, R.J. (eds.), pp. 659-64, Kluwer Academic/Plenum Publishing Corporation: New York (2001).
45. Kotiluoto, P., Hiismäki, P., Auterinen, I., Seppälä, T. and Aschan, C. Shielding design and calculations for the Finnish BNCT facility In: Frontiers in Neutron Capture Therapy, Vol. 1, Hawthorne, M.F., Shelly, K. and Wiersema, R.J. (eds.), pp. 623-8, Kluwer Academic/Plenum Publishing Corporation: New York (2001).
46. Nigg, D.W. and Wheeler, F.J. Preconceptual performance estimate for an epithermal-neutron beam for boron neutron capture therapy at the General Atomics Mark I Triga

facility in San Diego. EGG-NRE-11476, Idaho National Engineering Laboratory: Idaho (1994).
47. Peltonen, J. Loading scheme calculations of the Triga core for the BNCT unit using the MCNP model. VTT Energy: Espoo (1996) (In Finnish).
48. Nigg, D.W., Wemple, C.A., Serén, T., Seppälä, T. and Auterinen, I. Improved evaluation of the free-beam spectrum of the FiR 1 clinical epithermal-neutron beam facility for BNCT. In: INEEL BNCT Research Program Annual Report 2000, INEEL-EXT-01-00204, Venhuizen, J.R. (ed.), pp. 53-69, Idaho National Engineering and Environmental Laboratory: Idaho (2001).
49. Rogus, R.D., Harling, O.K. and Yanch, J.C. Mixed field dosimetry of epithermal neutron beams for boron neutron capture therapy at the MITR-II research reactor. Med. Phys. 21, 1611-25 (1994).
50. Wheeler, F.J., Nigg, D.W., Capala, J., Watkins, P.R., Vroegindeweij, C., Auterinen, I., Seppälä, T. and Bleuel, D. Boron neutron capture therapy (BNCT): implications of neutron beam and boron compound characteristics. Med. Phys. 26, 1237-44 (1999).
51. ICRU 45, Clinical Neutron Dosimetry Part I: Determination of Absorbed Dose in a Patient Treated by External Beams of Fast Neutrons. International Commission on Radiation Units and Measurements: Bethesda, Maryland (1989).
52. Liu, H.B., Greenberg, D.D., Capala, J. and Wheeler, F.J. An improved neutron collimator for brain tumor irradiations in clinical boron neutron capture therapy. Med.Phys. 23, 2051-60 (1996).
53. Raaijmakers, C.P., Konijnenberg, M.W., Verhagen, H.W. and Mijnheer, B.J. Determination of dose components in phantoms irradiated with an epithermal neutron beam for boron neutron capture therapy. Med. Phys. 22, 321-9 (1995).
54. Raaijmakers, C.P., Nottelman, E.L. and Mijnheer, B.J. Phantom materials for boron neutron capture therapy. Phys. Med. Biol. 45, 2353-61 (2000).
55. Kocherov, N.P. and McLaughlin, P.K., The International Reactor Dosimetry File (IRDF-90) (1993).
56. Tanner, V., Auterinen, I., Helin, J., Kosunen, A. and Savolainen, S. On-line neutron beam monitoring for the Finnish BNCT facility. Nucl. Instr. Meth. Phys. Res. A 422, 101-5 (1999).
57. Wessol, D.E., Wemple, C.A., Wheeler, F.J., Cohen, M.T., Rossmeier, M.B. and Cogliati, J., SERA: Simulation Environment for Radiotherapy Applications User's Manual Version 1C0. http://www.cs.montana.edu/~bnct/, INEEL External Report (2001).
58. Vroegindeweij, C., Watkins, P., Aaldijk, P. and Raaijmarkers, N. Definitions in the INEL treatment planning program and in the measurements for BNCT. HFR/97/4415, HFR: Petten (1997).
59. Wemple, C., INEEL, Idaho Falls, USA (private communication, 2002).
60. Seppälä, T., Kankaanranta, L., Serén, T., Auterinen, I., Joensuu, H. and Savolainen, S. BNCT_RTPE and SERA Dose Planning Programs: Phantom and Patient Studies. In: Program and abstracts of 9th International Symposium on Neutron Capture Therapy for Cancer, October 2-6, 2000, pp. 175-6. ISNCT: Osaka (2000).
61. Wessol, D.E., Wemple, C.A., Wheeler, F.J., Cohen, M.T., Rossmeier, M.B., Cogliati, J.J., Harkin, G.J. Venhuizen, J.R. and Nigg, D.W. Radiation treatment planning software development and deployment. In: INEEL BNCT Research Program Annual Report 1999, INEEL-EXT-2000-00392, Venhuizen, J.R. (ed.), pp. 6-16, Idaho National Engineering and Environmental Laboratory: Idaho (2000).

62. Karila, J., Aschan, C., Serén, T., Kotiluoto, P., Seppälä, T., Toivonen, M., Kankaanranta, L., Joensuu, H., Auterinen, I. and Savolainen, S. In vivo dosimetry for BNCT. In: Program and abstracts of 9th International Symposium on Neutron Capture Therapy for Cancer, October 2-6, 2000, pp. 117-8. ISNCT: Osaka (2000).
63. Savolainen, S., Auterinen, I., Aschan, C., Hiismäki, P., Kortesniemi, M., Kosunen, A., Kotiluoto, P., Lampinen, J., Seppälä, T., Seren, T., Tanner, V. and Toivonen, M. Dosimetry chain for the dogs irradiated in the epithermal neutron beam at the Finnish BNCT Facility. In: Frontiers in Neutron Capture Therapy, Vol. 2, Hawthorne, M.F., Shelly, K. and Wiersema, R.J. (eds.), pp. 1245-50, Kluwer Academic/Plenum Publishing Corporation: New York (2001).
64. Vroegindeweij, C., Watkins, P., Hideghety, K. and Sauerwein, W. Treatment planning for the first group of patients in the European glioma trial at HFR Petten. In: Frontiers in Neutron Capture Therapy, Vol. 1, Hawthorne, M.F., Shelly, K. and Wiersema, R.J. (eds.), pp. 153-9, Kluwer Academic/Plenum Publishing Corporation: New York (2001).
65. Brooks, R.A., DiChiro, G. and Keller, M.R. Explanation of cerebral white-gray contrast in computed tomography. J. Comp. Assist. Tomog. 4, 489-91 (1980).
66. Wojnecki, C. and Green, S. A computational study into the use of polyacrylamide gel and A-150 plastic as brain tissue substitutes for boron neutron capture therapy. Phys. Med. Biol. 46, 1399-1405 (2001).

ISBN 952-10-0569-6
ISSN 0356-0961
Helsinki 2002
Yliopistopaino